The Effect of Internucleosomal Interaction on Folding of the Chromatin Fiber

René Stehr,* Nick Kepper,† Karsten Rippe,† and Gero Wedemann*
*University of Applied Sciences Stralsund, System Engineering and Information Management, 18435 Stralsund, Germany; and †Deutsches Krebsforschungszentrum & BioQuant, Research Group Genome Organization & Function, 69120 Heidelberg, Germany

ABSTRACT The folding of the nucleosome chain into a chromatin fiber modulates DNA accessibility and is therefore an important factor for the control of gene expression. The fiber conformation depends crucially on the interaction between individual nucleosomes. However, this parameter has not been accurately determined experimentally, and it is affected by posttranslational histone modifications and binding of chromosomal proteins. Here, the effect of different internucleosomal interaction strengths on the fiber conformation was investigated by Monte Carlo computer simulations. The fiber geometry was modeled to fit that of chicken erythrocyte chromatin, which has been examined in numerous experimental studies. In the Monte Carlo simulation, the nucleosome shape was described as an oblate spherocylinder, and a replica exchange protocol was developed to reach thermal equilibrium for a broad range of internucleosomal interaction energies. The simulations revealed the large impact of the nucleosome geometry and the nucleosome repeat length on the compaction of the chromatin fiber. At high internucleosomal interaction energies, a lateral self-association of distant fiber parts and an interdigitation of nucleosomes were apparent. These results identify key factors for the control of the compaction and higher order folding of the chromatin fiber.

INTRODUCTION

In the cell nucleus of higher-order organisms, the DNA is wrapped around a histone protein core. The resulting protein-DNA complex is referred to as the nucleosome and represents the basic unit of chromatin (1). The nucleosomes are connected via the intervening linker DNA and form a beads-on-a-string-like structure that can associate into a fiber with a diameter of ~30 nm (1,2). The organization of this 30 nm fiber determines DNA accessibility and is therefore an important parameter for controlling gene expression (2–5). Although the structure of the nucleosome is known at atomic resolution (6–8), the structure of the fiber and its higher order organization remain controversial, and various models for the fiber geometry are still under investigation. The so-called solenoid model was reported two decades ago (9,10). Since then, numerous structures were proposed and investigated (1,11–25) and geometrically possible fiber conformations were systematically evaluated in phase diagrams using a two-angle model to describe the nucleosome geometry (26,27).

A critical feature of the solenoid model is the interaction between consecutive nucleosomes on the DNA chain. This requires significant bending of the intervening linker DNA, which could be facilitated by association with linker histone H1 (28). However, as linker DNA bending is energetically unfavorable, a number of fiber models with straight linker DNA have been proposed (29). These include two-start fiber models, in which neighboring nucleosomes on the DNA are oriented on different sides of the fiber with their connecting linker DNA crossing the inner section so that internucleosomal contacts are made between nucleosomes at positions i and $i + 2$ (24). The experimental data currently available support the view that at least three main types of different fiber conformations exist:

i. A two-start fiber helix that can be derived from the crystal structure of a tetranucleosome particle (20). This structure has a short nucleosome repeat length of 169 bp and was determined in the absence of linker histones.
ii. A one-start helix with interdigitated nucleosomes (14,19) as derived recently from electron microscopy studies of chromatin fibers reconstituted in vitro with longer repeat lengths (177–237 bp) and one linker histone per nucleosome (19).
iii. A two-start helix conformation with crossed-linker DNA as proposed on the basis of electron microscopy studies of native chromatin fibers extracted from chicken erythrocytes. These showed a zig-zag-like DNA backbone with a so-called nucleosome stem motif (13,30). In this nucleosome stem, the linker histone H5 mediates the association of the two DNA segments, leaving the nucleosome core particle over a distance of 3–5 nm before the linker DNA diverges. This type of fiber will be analyzed in further detail here, whereas the first two have been the subject of our accompanying study (16).

A crucial parameter for assessing the stability of different fiber conformations is the interaction energy between nucleosomes, since this is the driving force for the compaction of the nucleosome chain. Based on stretching experiments of native chromatin fibers isolated from chicken erythrocytes, Cui and Bustamante determined an apparent mean interac-

Submitted August 29, 2007, and accepted for publication July 1, 2008.

Address reprint requests to Gero Wedemann, University of Applied Sciences Stralsund, Zur Schwedenschanze 15, 18435 Stralsund, Germany. Tel.: 49-3831-457051; Fax: 49-3831-45712051; E-mail: gero.wedemann@fh-stralsund.de.

Editor: Klaus Schulten.

0006-3495/08/10/3677/15 $2.00

doi: 10.1529/biophysj.107.120543

tion energy of ~3.4 kT per nucleosome (31). More recently, a force spectroscopy study of nucleosome arrays reconstituted with recombinant histones reported an interaction energy of up to 10–16 kT per nucleosome (32). Thus, the specific fiber composition could result in large differences of the nucleosome-nucleosome interaction energy. In this context, the linker histones could play an important role since full compaction of the chromatin fiber requires their incorporation at a ratio of one H1 (or H5) per nucleosome (19). As discussed previously, the linker histone binding changes the local nucleosome geometry and neutralizes negative charges in the linker DNA (16). In addition, H1/H5 binds cooperatively to DNA and contains at least two DNA binding sites (33,34). Thus, it could directly be involved in mediating DNA-DNA, DNA-protein, and protein-protein associations that stabilize the stacking of nucleosomes in a compacted fiber. Nucleosome-nucleosome interactions are also affected by posttranslational histone modifications. From atomic force microscopy studies of nucleosome arrays, an energy difference of 0.4 kcal mol^{-1} (equivalent to 0.7 kT) was predicted between acetylated and unacetylated nucleosomes (35). Similar effects were observed by acetylating H4 on lysine 16, which inhibits the formation of compact nucleosome arrays, indicative of a decrease of the interaction energy between nucleosomes (36).

Furthermore, chromatin architectural proteins, for example MeCP2, the polycomb complex, or heterochromatin protein 1 (HP1), are known to promote the condensation of chromatin (37,38). Results from experimental studies indicate that some of these proteins maintain lateral and longitudinal bridging of nucleosomes, which increases the internucleosomal interaction strength (37). The magnitude of this contribution can be estimated for HP1 from its binding affinity. In vivo, the dissociation constant of HP1 to a single nucleosome is in the low micromolar range, and thus corresponds to a binding energy of ~10 kT per molecule, with HP1 being present at a concentration of ~10 μM in the nucleus (39,40). Since HP1 protein associates into a dimer, it could serve as a linker between two adjacent nucleosomes and stabilize their stacking interaction (37,39). Hence, the internucleosomal interaction in vivo is not a constant value but can be strongly modulated by histone (de)acetylation and/or the binding of chromosomal proteins over an estimated range of at least ~10 kT. Finally, it is well known that the 30 nm fiber decondenses into a beads-on-a-string-like chain when lowering the salt concentration to 10 mM and below (29,41–44). Sun et al. evaluated this salt dependence of the electrostatic energy between DNA linkers and nucleosomes in computer simulations (21). Raising the salt concentration from 10 mM to 100 mM decreased the repulsion between DNA linkers and increased the attraction energy between nucleosomes with a total of energy difference of 54 kcal mol^{-1} for a 12-nucleosome array (equivalent to 2.7 kT per nucleosome). Such a salt-dependent transition from repulsive to attractive interactions between nucleosomes was also observed in small angle x-ray scattering experiments (45).

The aforementioned findings demonstrate that the energetics of nucleosome-nucleosome interactions is an essential determinant of the chromatin fiber structure. By applying Monte Carlo (MC) simulations, a representative ensemble of chromatin fiber configurations at thermal equilibrium can be computed to evaluate the stability of a given fiber conformation. This approach has been used successfully in previous studies to investigate the salt-dependent compaction of the chain, the role of histone tails, the effect of linker histone binding, and to simulate the stretching of the chromatin fiber (11,12,16,18,21,22,46). Here, MC simulations of nucleosome chains were conducted to evaluate the impact of the internucleosomal interaction strength on the folding of the chromatin fiber for chains composed of 100 nucleosomes. A nucleosome potential, which describes the nucleosome as a spherocylinder, and a replica exchange protocol were developed to reach thermal equilibrium for a broad range of internucleosomal interaction strength. The simulations were conducted with a model for chromatin from chicken erythrocytes as derived from experimental data. This model was used to investigate the influence of the nucleosome-nucleosome interaction for different nucleosome geometries and repeat lengths. The results identified the impact of the nucleosome geometry and the nucleosome repeat length on the conformation of the chromatin fiber. Furthermore, the internucleosomal interaction strength was found to be a key factor for the control of compaction and higher order folding of chromatin.

MATERIALS AND METHODS

Chromatin fiber model

The description of the chromatin fiber used here shares a number of features with a chromatin fiber model previously introduced by Wedemann and Langowski (22): The fiber is approximated by a coarse-grained model based on the ''two-angle'' model (24) (Fig. 1 *A*). According to experimental data (13,20), the nucleosomes are connected by linker DNA, modeled as cylindrical segments with a diameter of 2 nm. Harmonic potentials for stretching, bending, and torsion represent the elastic properties of the DNA. Due to the negative charge of the DNA, the DNA-DNA interaction is described by a Debye-Hückel-approximation (22). The excluded volume of DNA and nucleosomes is described by a hard core potential. To consider the influence of the linker histone, a stem structure was included in the model (13,30). The distance c between the nucleosome center and the connection point of the linker DNA was increased to 8 nm, which results in a distance of 22 bp between the exit point of DNA at the stem and the core particle. Thus, the total nucleosome repeat length (NRL) consists of 146 bp DNA wrapped 1.67 turns around the core particle and 2 × 22 bp of DNA between the stem and the connection point at the core particle, yielding 190 bp plus the length of the linker DNA. For chicken chromatin fibers, the nucleosome repeat length is 212 bp (1) so that the length of the linker DNA is 22 bp.

Internucleosomal potentials

In previous studies, internucleosomal interactions based on hard spheres (15,47) or ellipsoids with the Gay-Berne potential (18,22,46) have been used to model internucleosomal interactions. However, observations of the crystal structure of the nucleosome suggest that the shape of the nucleosome is more

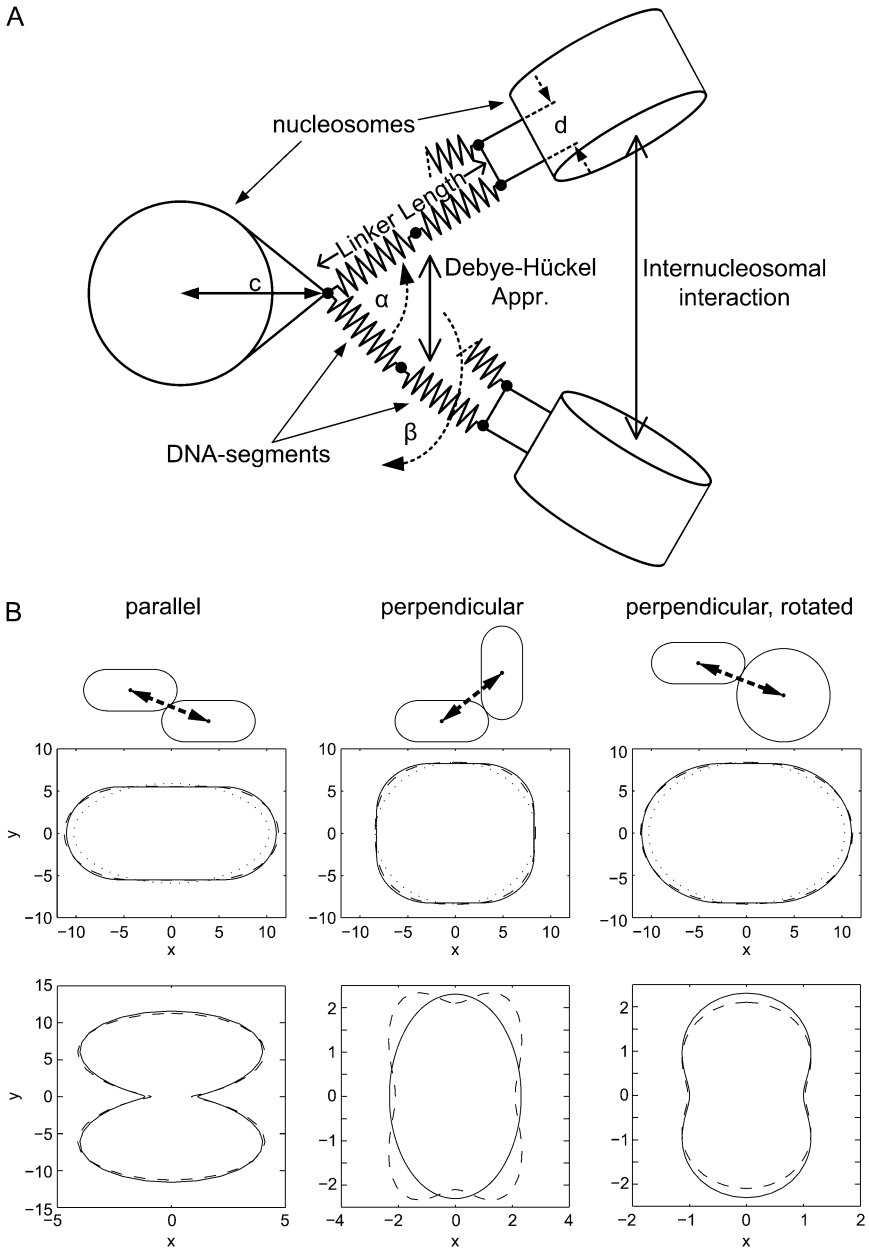

FIGURE 1 Chromatin fiber model. (*A*) Schematic description of the computer simulation model. It consists of cylindrical-shaped nucleosomes, which are connected by elastic DNA segments. The model is based on the ''two-angle'' model (24) where the fiber is parameterized by the linker length, the opening angle α of the linker DNA, and the twisting angle β between consecutive nucleosomes. Furthermore, the presence of the linker histone was accounted for by a stem structure (13,30) that is described by the distance c between the nucleosome center and the entry-exit point of the DNA segments. The negative charge of the DNA is described by a Debye-Hückel approximation, whereas the internucleosomal interaction is described by shifted Lennard-Jones potentials. (*B*) Comparison of the range parameter σ (*first row*) and the strength parameter ε (*second row*) for three nucleosome potential models: hard oblate spherocylinder (*solid line*), oblate ellipsoids described by Gay-Berne (*dotted line*), and spherocylinders described by S-functions (*dashed line*). (*Left column*) Parallel orientation with $f_0 = 0$, $f_1 = f_2 = \cos\phi$, (*center column*) perpendicular orientation with $f_0 = f_2 = 0, f_1 = \cos\phi$, and (*right column*) perpendicular orientation (*rotated*) with $f_0 = 0$, $f_1 = \cos\phi$, $f_2 = \sin\phi$.

realistically described as a cylinder (6,20). To study the effect of different nucleosome shapes on fiber conformation, three shapes were investigated: spheres described by a 12-6 Lennard-Jones potential, oblate ellipsoids described by a modified Gay-Berne potential (22), and spherocylinders described by an S-functions expansion referred to as Zewdie potential (48,49).

The Gay-Berne potential and the Zewdie potential are defined as

$$U(\hat{u}_1,\hat{u}_2,\vec{r}) = 4\,\varepsilon(\hat{u}_1,\hat{u}_2,\hat{r})\left[\left(\frac{\sigma_0}{r-\sigma(\hat{u}_1,\hat{u}_2,\hat{r})+\sigma_0}\right)^{12} - \left(\frac{\sigma_0}{r-\sigma(\hat{u}_1,\hat{u}_2,\hat{r})+\sigma_0}\right)^{6}\right] \quad (1)$$

with $\hat{u}_1$ and $\hat{u}_2$ as unit vectors describing the orientation of the particles and $\vec{r}$ as the vector of the distance of the particles. For the Zewdie potential, the potential range σ and strength ε are replaced by anisotropic S-functions for identical cylindrically symmetric particles. The potential range is defined as

$$\sigma(\hat{u}_1,\hat{u}_2,\hat{r}) = \sigma_0[\sigma_{000}S_{000} + \sigma_{cc2}(S_{202}+S_{022}) + \sigma_{220}S_{220} + \sigma_{222}S_{222} + \sigma_{224}S_{224}] \quad (2)$$

and the potential strength is given by

$$\varepsilon(\hat{u}_1,\hat{u}_2,\hat{r}) = \varepsilon_0[\varepsilon_{000}S_{000} + \varepsilon_{cc2}(S_{202}+S_{022}) + \varepsilon_{220}S_{220} + \varepsilon_{222}S_{222} + \varepsilon_{224}S_{224}]. \quad (3)$$

In Eqs. 2 and 3, ε_0 and σ_0 scale the potential strength and the potential range, respectively. For details of the range and strength parameters of the Gay-Berne potential, see Wedemann and Langowski (22). For the spherical-shaped nucleosome, the strength and range functions of the Gay-Berne potential were parameterized isotropically. The S-functions for the Zewdie

potential are given in Table 1. To choose the expansion coefficients for the range and strength functions of the spherocylinders, the approach described by Zewdie (49) was used for a spherocylinder with a 5.5 nm radius and 5.5 nm height. The expansion coefficients of the shape function were determined by performing a least-square fit of Eq. 2 to this function (Fig. 1 *B*, *first row*). Since the spatial dependency of the strength function is not known in detail, the expansion coefficients were determined by a least-square fit of Eq. 3 to the strength function of the corresponding Gay-Berne-potential (Fig. 1 *B*, *second row*). Since the potentials for ellipsoidal and spherocylindrical-shaped nucleosomes are anisotropic, the internucleosomal interaction strength E_{max} is defined as the minimal energy value of two elements.

Simulation procedures

The classical Metropolis-Monte Carlo algorithm is a standard procedure to create a statistically relevant set of configurations satisfying the Boltzmann distribution (50). An ensemble of fiber configurations that represents the thermal equilibrium distribution is referred to as trajectory. Different configurations were generated with rotation and pivot moves (51,52). Results of preparative simulations indicated that some structures with $E_{max} > 3\ kT$ did not reach equilibrium even after several millions of simulation steps and that the correlation length was very high (data not shown). To avoid this problem, a replica exchange procedure was used. This is the common form of the parallel tempering procedure introduced by Swendsen and Wang to reduce the correlation times of Monte Carlo simulations of spin glasses (53), which was subsequently applied in several studies (54–57). For the application of this approach here, M replicas of the original system were simulated simultaneously, each at a certain temperature, T_i. After a defined number of MC simulation steps, the systems of adjacent temperatures (T_i, T_{i+1}) attempted to exchange their replicas with the probability

$$\min[1, \exp(-(\beta_i - \beta_{i+1})(E_{i+1} - E_i))], \tag{4}$$

where $\beta_i = 1/(k_B T_i)$, with k_B the Boltzmann's constant and E_i the energy of the system i. Thus, the systems simulated were heated up and cooled down in a random manner, which allowed the systems to escape from local energy minima.

The performance of the replica exchange algorithm was found to depend on the selection of the number of replicas and the temperatures (58,59). For a fixed lowest temperature, the highest temperature must be sufficiently high to allow escape from local minima in the energy landscape. Furthermore, the number of replicas must be large enough to achieve sufficient swap probabilities among all adjacent temperatures. The feedback-optimized approach of Katzgraber et al. was utilized to determine the temperatures at a given maximum temperature (58). This algorithm localizes computation bottlenecks, e.g., caused by phase transitions, by measuring the local diffusivity of the replica exchange simulation. Therefore, an ''up'' or ''down'' label was assigned to each replica, which indicated if a replica was currently heating up or cooling down, respectively. The label changed only if a replica had reached the opposite temperature (T_1 or T_M). From these labels, two histograms $n_{up}(T_i)$ and $n_{down}(T_i)$ for each temperature T_i were derived. Before temperature swaps, the histograms were updated. For each temperature point, the fraction of replicas, which reached the minimum temperature, was determined:

$$f(T) = \frac{n_{up}(T)}{n_{up}(T) + n_{down}(T)}. \tag{5}$$

Following Katzgraber et al. (58), the optimized probability distribution for the continuous variable T was defined as

$$\eta'(T) = C' \sqrt{\left| \frac{1}{\Delta T} \frac{df}{dT} \right|}, \tag{6}$$

where $\Delta T = T_{i+1} - T_i$ is the length of the interval $T_i < T < T_{i+1}$ and C' was chosen so that

$$C' \int_{T_1}^{T_M} \eta'(T) = 1. \tag{7}$$

By linear regression of the discrete values of Eq. 5, the value of df/dT was determined. The optimized temperature set $\{T'_i\}$ was then found by choosing the kth temperature T'_k such that

$$\int_{T_1}^{T'_k} \eta'(T) dT = \frac{k}{M-1}. \tag{8}$$

This optimization was repeated until the temperature set converged. Since the energy distribution and therefore the local diffusivity of relaxed and nonrelaxed conformations deviated strongly, it is unfavorable to determine the temperatures during the relaxation progress. To speed up the relaxation of the conformation, a simulated annealing approach was performed (60). The resulting fiber was then chosen as the start configuration to compute the temperatures to be used in the final replica exchange simulations. The replica exchange simulations were conducted with a target temperature of 293 K. The highest temperature was chosen to allow the fiber a complete reorganization of the structure. Based on visual inspections, maximum temperatures of 550 K with 16 temperatures, 700 K with 32 temperatures, and 850 K with 64 temperatures were selected for E_{max} values of 6, 9, and 12 kT, respectively. In simulations using the potential for spherical-shaped nucleosomes, the simulated structures exhibited compact condensed structures at $E_{max} > 0.5\ kT$ and formed blob-like structures at higher interaction strength. In this case, the replica exchange method was already used for $E_{max} > 0.5\ kT$ with a maximum temperature of up to 750 K for $E_{max} = 1.5\ kT$.

TABLE 1 First six S-functions for identical cylindrically symmetric particles. $\hat{u}_1$ and $\hat{u}_2$ are the unit vectors defining the orientation of the particles and $\hat{r}$ is the unit vector of the distance of the particles

$$f_0 = \hat{u}_1 \cdot \hat{u}_2, f_1 = \hat{u}_1 \cdot \hat{r}, f_2 = \hat{u}_2 \cdot \hat{r}.$$

$$S_{000} = 1, S_{202} = (3f_1^2 - 1)/2\sqrt{5}, S_{022} = (3f_2^2 - 1)/2\sqrt{5}, S_{220} = (3f_0^2 - 1)/2\sqrt{5},$$

$$S_{222} = (2 - 3f_1^2 - 3f_2^2 - 3f_0^2 + 9f_1f_2f_0)/\sqrt{70},$$

$$S_{224} = (1 + 2f_0^2 - 5f_1^2 - 5f_2^2 - 20f_0f_1f_2 + 35f_1^2f_2^2)/4\sqrt{70}$$

Analysis parameters

The trajectories were analyzed in terms of their linear mass density, the persistence length (determined as described in Wedemann and Langowski (22)), the global shape of the chromatin chain, and the number of interdigitated nucleosomes. The linear mass density μ is defined as the ratio of the number of nucleosomes N_n to the contour length of the chain l_c:

$$\mu = \frac{N_n}{l_c}, \tag{9}$$

where the contour length l_c is given by

$$l_c = \sum_{i=2}^{N_c} |\vec{c}_i - \vec{c}_{i-1}|, \tag{10}$$

with $\vec{c}_i$ the center point of the backbone of the fiber and N_c the number of calculated center points. The center points of the backbone were determined from

$$\vec{c}_i = \frac{1}{N_w}\sum_{j=1}^{N_w}\vec{R}_{j+(i-1)N_s},\ i = 1,\ldots,\left\lfloor\frac{N-N_w}{N_s}+1\right\rfloor. \quad (11)$$

N is the number of beads of the chain and the window size N_w is the number of beads that are averaged at one center point. N_s is the step width for moving the averaging window along the chain and $\vec{R}_j$ is the center of the bead j. A window size N_w of 40 beads and a step width N_s of 5 beads were chosen in the analysis.

To evaluate the fiber shape, three different approaches were used:

i. The fiber shape coefficient (FSC) that describes the overlap between distant chain regions was computed. The shape of the entire chain was approximated as a series of spheres. The sphere of a region i is described by its center point $\vec{c}_i$ and its radius r_i (Fig. S1 *A* in the Supplementary Material, Data S1). The center point is defined in Eq. 11 and the sphere radius r_i of a chain region is defined as the maximum distance between the center point of the sphere and the most distant of the N_w beads belonging to this sphere. The number of all beads, which are inside the sphere of the region i, is defined by in_i (the N_w beads defining the sphere plus possibly additional beads belonging to not directly subsequent fiber parts). The nonoverlap coefficient (noc_i) is defined as the ratio of the number of beads, which belong directly to the sphere i, to the number of all beads, which are actually inside this sphere:

$$noc_i = \frac{N_w}{in_i}. \quad (12)$$

Therefore, this coefficient indicates if a chain region overlaps with other regions. The *noc* value is 1 if the current chain region does not overlap with other regions and is ~0.5 if the number of distant beads is equal to the number of adjacent beads, which define the current region (Fig. S1 *B*, Data S1). The FSC value is defined as the mean of the nonoverlap coefficient of all considered spheres.

ii. A principal components analysis (PCA) was applied as described by Kepper et al. (16). The ratio of the longest and shortest half axis of a scalene ellipsoid, which was fitted to the nucleosome center of the configuration, was determined from the eigenvalues of the covariant matrix. A spherical volume yields a PCA ratio of 1, whereas a PCA ratio >3 was used here to classify a trajectory as fiber-shaped.

iii. The radius of gyration was determined to characterize the volume of the nucleosome chain according to Eq. 13:

$$R_G^2 = \frac{1}{N_n}\sum_{i=1}^{N_n}(\vec{n}_i - \langle\vec{n}\rangle), \quad (13)$$

where $\vec{n}_i$ is the center point of nucleosome i.

The degree of interdigitation was determined from the number of nucleosomes that were incorporated in distant fiber parts. A nucleosome was marked as interdigitated if it had two neighbors, which had a minimum genomic distance of 10 nucleosomes and a maximum center-to-center distance of 8 nm to the nucleosome of interest.

Correlation lengths and number of simulation steps

To calculate the number of uncorrelated configurations and to compute errors, the correlation times were determined from the autocorrelation function as described (22). The autocorrelation function was calculated for energy, end-to-end distance, PCA ratio, FSC, and linear mass density. The maximum autocorrelation time was calculated for a typical configuration (see below). Simulations with all nucleosome potentials and several E_{max} values were performed and the maximum correlation length for each combination was determined. For simulations performed with replica exchange, the maximum autocorrelation time of all simulated trajectories was selected. For analysis, the first 100 statistically independent configurations were not considered to avoid a bias toward the start structure. We performed 1.5×10^7, 2×10^7, 2×10^7, 1×10^8, and 1.2×10^8 MC steps for E_{max} of 1.5, 3, 6, 9, and 12 *kT*, respectively, corresponding to 275–500 statistically independent configurations.

Simulation parameters

The MC simulations were conducted with the parameters listed in Table 2 and Table S1 (Data S1). The elastic parameters were chosen as described by Wedemann and Langowski (22). For the DNA, the values are based on the average of experimentally determined values of 45–50 nm DNA bending persistence length and a DNA torsion elasticity of $2.8 \pm 0.2\times10^{-19}$ J nm (61). The elasticity of the chromatosome has not been derived from experimental studies. Therefore, values were chosen that essentially maintain the initial conformation of the chromatosome.

Based on single-fiber stretching experiments, a nucleosome-nucleosome attraction energy of ~3.4 *kT* has been reported (31). From previous MC simulations, an interaction energy E_{max} of 6 *kT* was found to result in an effective energy E_{eff} of ~3.5 *kT* between nucleosomes in the context of a tetranucleosome structure (16), and a standard value of $E_{max} = 6\ kT$ was used here. The anisotropy of the potential was described by the ratio $E_{lateral}/E_{longitudinal}$ between the interaction strength of lateral- and longitudinal-oriented nucleosomes of the Gay-Berne potential and the Zewdie potential (22). For this ratio, the value of 1/6 was chosen for E_{max} of up to 1.5 *kT*, as it has been used in previous works (22,46). Thus, an E_{max} value of 1.5 *kT* for ellipsoids and spherocylinders corresponds to $\varepsilon_0 = 0.25\ kT$ (see Eq.3). Simulations with $E_{max} > 1.5\ kT$ yielded structures, with a strong tendency to fold back (data not shown). To avoid this behavior, which was caused by unrealistically high lateral attractions, this ratio was decreased to 1/12 for E_{max} values >1.5 *kT*. For the parameterization of the spherical potential, E_{max} is directly defined by ε_0.

Although the actual value of the ratio $E_{lateral}/E_{longitudinal}$ has not been determined experimentally, the anisotropic parameterization of the internucleosomal potential makes the aligned stacking of two nucleosome cylinders the most stable geometry in agreement with a number of experimental studies. These include the tetranucleosome crystal structure (20) and the arrangement found in liquid crystals of nucleosome core particles (reviewed by Livolant et al. (62)), as well as the observation of ribbon-like structures of nucleosome stacks by electron microscopy images of intact, nuclease-isolated chromatin fibers (63) and cross-linked nucleosome arrays (64). Furthermore, determinations of nucleosome nearest neighbor distributions derived from atomic force microscopy images of nucleosome arrays yielded

TABLE 2 Parameters of the nucleosome-nucleosome potentials

Potential	Parameter/value	
Gay-Berne (sphere)	$\sigma_0 = 10.3$ nm	
	$\chi = 0$	
	$\chi' = 0$	
	$E_{lateral}/E_{longitudinal} = 1/6$	$E_{lateral}/E_{longitudinal} = 1/12$
Gay-Berne (ellipsoid)	$\sigma_0 = 10.3$ nm	$\sigma_0 = 10.3$
	$\chi = -0.506$	$\chi = -0.506$
	$\chi' = -0.383$	$\chi' = -0.519$
Zewdie (spherocylinder)	S000 = 1.6957	S000 = 1.6957
	Scc2 = −0.7641	Scc2 = −0.7641
	S220 = −0.1480	S220 = −0.1480
	S222 = −0.2582	S222 = −0.2582
	S224 = 0.5112	S224 = 0.5112
	E000 = 1.9152	E000 = 2.7206
	Ecc2 = 2.7322	Ecc2 = 6.0995
	E220 = 1.2633	E220 = 3.3826
	E222 = 2.3440	E222 = 7.1036
	E224 = 1.0101	E224 = 3.2870
	$\sigma_0 = 5.5$ nm	$\sigma_0 = 5.5$ nm

also evidence in support of a stacking of nucleosomes at physiological salt conditions (35,65).

Simulation software

The simulation program was adapted for the use of shared memory parallel architectures according to the OpenMP standard, and the replica exchange algorithm was implemented for distributed memory architectures using Message Passing Interface. The algorithm was verified with an extensive set of unit tests and tests using simplified chain models with stretching modulus only and with additional bending and torsion energies, which reproduced the expected analytical values. In addition to run-time checks and automated unit tests (22), Polyspace for C++ and Rational Purify for Linux were used as static and dynamic code analysis tools, respectively, for error checks. Computations were done on a Linux cluster (Intel Xeon 3.2 GHz) and on the parallel supercomputer (IBM pSeries 1.3Ghz Power4) at the North German Supercomputing Alliance (HLRN). A single simulation (without replica exchange) on a single core processor with 1 million MC steps took between ~0.75 h (Linux Cluster) and ~2 h (HLRN). Replica exchange simulations with n temperatures on n processor cores required approximately the same computation time, yielding a total of ~8 years single processor time for the simulations presented here.

RESULTS

A coarse-grained description of chromatin from chicken erythrocytes

In studies of chromatin from chicken erythrocytes, nucleosomes display a characteristic stem structure of the DNA induced by the binding of linker histone H5 (13,30). This structure was modeled by including an additional distance between the nucleosome center and the DNA connection point, and appropriate values for the linker DNA entry-exit angle α at the stem and the nucleosome twist angle β were chosen (Fig. 1 *A*). An opening angle α of 26° led to an equilibrium value of ~35° for this parameter (22), which is in very good agreement with the experimental reported value of ~35° for chromatin from chicken erythrocytes under physiological salt concentration (80 mM M^+) (13). As NRL, the value of 212 bp was chosen according to the experimental determinations for chicken erythrocytes (1). Since the nucleosome twist angle β has not been directly determined in the experiments, the effect of different β-values was evaluated in the simulations (see below).

A potential describing spherocylindrical-shaped nucleosomes is required for the formation of chromatin fibers at physiological internucleosomal interaction strength

The influence of different nucleosome potentials was investigated with simulations for a range of E_{max} values for the described conformation (see above) with $\beta = 80°$. With spherocylindrical-shaped nucleosomes, a folding of the nucleosome chain into stable fibers was obtained for E_{max} up to 6 kT (Fig. 2). Investigations of lower internucleosomal interaction strengths revealed that systems with spherical-shaped nucleosomes formed fiber structures for E_{max} up to 0.5 kT (data not shown) and with ellipsoidal-shaped nucleosomes for E_{max} up to 1.5 kT, whereas systems associated into aggregated structures for higher E_{max} values (Fig. 2).

To evaluate the differences between ellipsoidal- and spherocylindrical-shaped nucleosomes in further detail, simulations were conducted with variations of several parameters (α, β, NRL) at $E_{max} = 1.5\ kT$, and compared with respect to the linear mass density. The differences were found to be within the statistical error (data not shown). However, the FSC value differed strongly for both nucleosome shapes. Whereas at $E_{max} = 1.5\ kT$ both descriptions led to the formation of chromatin fibers (Fig. 2), the spherocylindrical-shaped nucleosomes appeared to yield more stable fibers (Table 3). The differences between both potentials increased at higher internucleosomal interaction strength (Fig. 2 *B*).

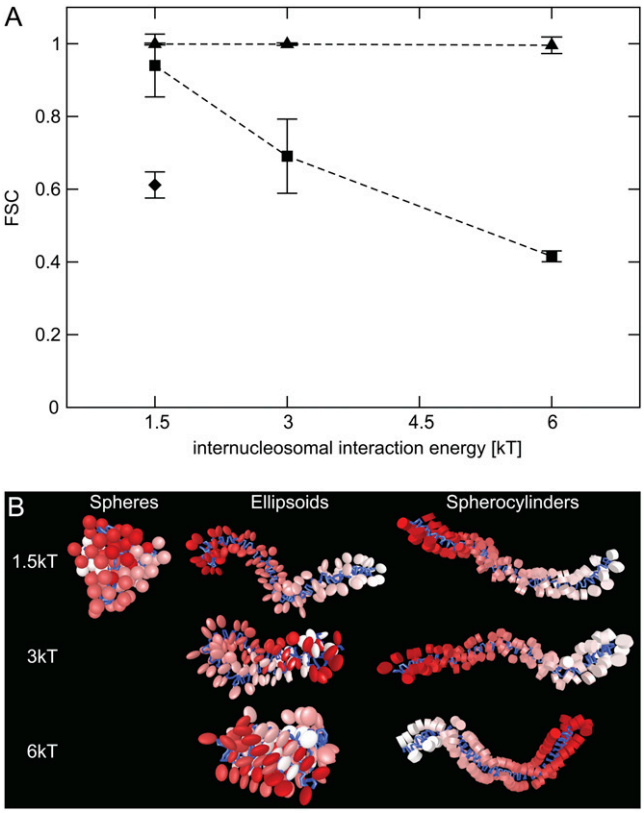

FIGURE 2 Influence of different internucleosomal potentials on the formation of chromatin fibers. Simulations were conducted for an example geometry with $\alpha = 26°$, $\beta = 80°$, NRL = 212 bp, and E_{max} values of 1.5, 3, and 6 kT. Systems with spherical-shaped nucleosomes built blob-like aggregates at $E_{max} = 1.5\ kT$, whereas ellipsoidal- and spherocylindrical-shaped nucleosomes form fiber structures. Ellipsoidal-shaped nucleosomes led to folded structures such as hairpins at $E_{max} = 3\ kT$ and formed compact condensed structures at $E_{max} = 6\ kT$. Systems with spherocylindrical-shaped nucleosomes built fiber structures for E_{max} up to 6 kT. (*A*) FSC values of structures with different nucleosome shapes: sphere (♦), ellipsoid (■), and spherocylinder (▲). The error bar is the standard deviation. (*B*) Visualizations of the simulated fiber. The nucleosomes are colored by their position in the chain (first is *white*, last is *red*) and the DNA segments are colored blue.

TABLE 3 FSC with standard deviation as a function of NRL for an example configuration ($\alpha = 26°$, $\beta = 80°$, and $E_{max} = 1.5\ kT$) of systems with ellipsoidal- and spherocylindrical-shaped nucleosomes

NRL (bp)	FSC (ellipsoid)	FSC (spherocylinder)
201	$1 \pm 7.33 \times 10^{-4}$	$1 \pm 3.9 \times 10^{-5}$
212	0.912 ± 0.109	$0.999 \pm 3.02 \times 10^{-3}$
223	0.849 ± 0.104	0.987 ± 0.019

Fibers with ellipsoidal-shaped nucleosomes folded back into hairpins and other structures at $E_{max} = 3\ kT$ and above (Fig. 2), whereas spherocylindrical-shaped nucleosomes led to stable fiber structures for E_{max} values of up to 6 kT. Since at this interaction strength neither the potential for spherical- nor for ellipsoidal-shaped nucleosomes was compatible with the folding of the nucleosome chain into a chromatin fiber, the spherocylindrical parameterized Zewdie potential was chosen for further investigations.

A replica exchange protocol is advantageous for evaluating the fiber conformation over a broad range of internucleosomal interaction energies

For simulations using replica exchange, a three-step protocol was developed to yield the best results in terms of reaching thermal equilibrium with efficient use of computation time:

i. To avoid a bias introduced by the start structure, a simulated annealing procedure was performed. Starting from a straight line, 10^6 MC steps were performed at the maximum temperature. The resulting configuration was subsequently cooled down in 5 K intervals, each with 5×10^5 MC steps until the lowest simulation temperature of 293 K was reached.
ii. In the second step, the appropriate temperatures for the replica exchange simulations were determined. The temperature set for the first replica exchange simulation was chosen by the approach of Rathore et al., which led to nearly uniform acceptance rates of temperature swaps between adjacent temperatures (59). Then the feedback-optimization process of Katzgraber et al. was applied to generate an optimized temperature set using preparative replica exchange simulations (see Materials and Methods) (58).
iii. For the final replica exchange simulations, temperature swaps were attempted every 2000 MC steps and acceptance rates of ~0.3 and 0.5 for the pivot and bead rotation moves, respectively, were reached. Since acceptance rates were found to be dependent on the simulation temperature, the rotation angle of both moves was chosen to be a function of the temperature.

To investigate the effectiveness of the replica exchange protocol, example fibers with E_{max} of 6, 9, and 12 kT were simulated with and without this protocol. The analysis of the energy of each fiber trajectory showed that in particular at $E_{max} > 6\ kT$, lower energy was obtained with the replica exchange protocol as compared to 5×10^7 Metropolis-MC simulation steps (Fig. 3). Moreover, inspection of the resulting three-dimensional (3D) structures at 9 and 12 kT indicated that the configurations simulated with standard Metropolis-MC did not fold into fiber structures. Blob-like aggregates as well as chain parts external to the folded fibers were observed (see visualizations in Fig. 3). Whereas at $E_{max} = 6\ kT$ many simulations with standard Metropolis-MC yielded the same results as the replica exchange protocol, some did not reach thermal equilibrium even after $5 \cdot 10^7$ simulation steps (Fig. 3). Furthermore, simulations of already relaxed systems at $E_{max} > 6\ kT$ yielded higher correlation lengths and these systems did not perform transitions to other structures (e.g., from hairpins to fiber structures) as observed for replica exchange simulations (see below). This indicates that the systems were not able to overcome barriers in the energy landscape.

Nucleosome twist angles in the range of 40–120° reproduce the conformation of the chicken chromatin fiber

To evaluate the effect of the twist angle β between consecutive nucleosomes, β was systematically varied in the range of −180–180° in steps of 20°. The results demonstrated a direct dependence of fiber conformation on β (Fig. 4, and Figs. S2 and S3, Data S1). The FSC values indicated the formation of fiber structures in the range of 40–120° (Fig. 4). The linear mass density had a maximum of ~4.8 nucleosomes/11 nm fiber at $\beta = 120°$. The PCA ratio was highest at ~5.7 for $\beta = 60°$ and the fiber diameter had a minimum of ~30.5 nm at $\beta = 100°$ (Fig. S3, Data S1). For further investigations of the chicken chromatin fiber conformation, a β-value of 100° was selected, which resulted in a high linear mass density (~4.6 nucleosomes/11 nm fiber), a fiber-like conformation with ~30 nm diameter, a FSC value of ~1, and a PCA ratio of 5.3.

Since the linker length of native chromatin fibers displays variations of 1–3 bp around an average value (1), the twist angle β is likely to vary significantly according to the helical twist of DNA of ~36° per basepair. Accordingly, simulations were conducted with a Gaussian distribution of β-values between each nucleosome pair. Five simulations, each with standard deviations σ of 0° (constant β), 10°, 20°, and 30°, were performed for E_{max} values of 1.5, 3, and 6 kT. For all simulations, the persistence length displayed a strong decrease with a broadening of the β-distribution and dramatically smaller, but significant, reduction of the PCA ratio and the radius of gyration were apparent (Table 4). The other analysis parameters remained essentially unchanged for $E_{max} \leq 3\ kT$. However, at $E_{max} = 6\ kT$, the FSC value decreased and the number of interdigitated nucleosomes increased somewhat (Table 4; Fig. S4, Data S1).

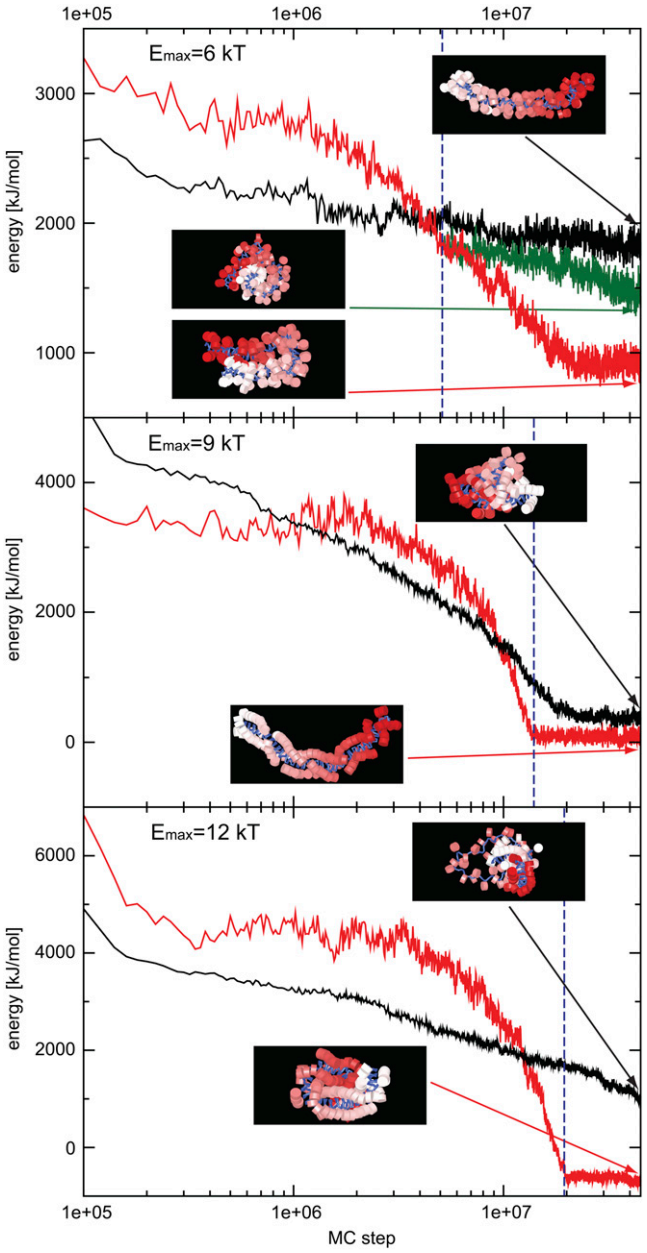

FIGURE 3 Comparison of the relaxation progress of structures simulated with and without the replica exchange protocol. Simulations for E_{max} of 9 and 12 kT were conducted with $\alpha = 26°$, $\beta = 100°$, and NRL = 212 bp, and for $E_{max} = 6\ kT$ with $\alpha = 26°$, $\beta = 160°$, and NRL = 212 bp. The replica exchange simulations were prepared by simulated annealing simulations (*dashed blue line* marks the end of these simulations). At $E_{max} = 6\ kT$ with replica exchange (16 temperatures, *green curve*) and with standard Metropolis-MC (*black curve*), the equilibrium was not reached even after 5×10^7 MC steps. However, for the replica exchange simulation with 32 temperatures, the equilibrium was reached after $\sim 2 \times 10^7$ MC steps (*red curve*). At $E_{max} = 9\ kT$, the replica exchange simulation with 32 temperatures (*red curve*) led to a significant lower energy than with standard Metropolis-MC (*black curve*). At $E_{max} = 12\ kT$, the structure simulated with standard Metropolis-MC (*black curve*) did not reach equilibrium even after 5×10^7 MC steps, whereas the structure simulated with the replica exchange protocol (*red curve*) already reached equilibrium after the simulated annealing simulation ($\sim 1.9 \times 10^7$ MC steps). In addition, visualizations of the resulting fibers after 5×10^7 MC steps revealed for simulations with standard Metropolis-MC at E_{max} of 9 and 12 kT the formation of blob-like aggregates as well as chain parts external to the folded fibers, whereas simulations with replica exchange yielded fiber-structures, which were in some cases folded, e.g., to hairpins.

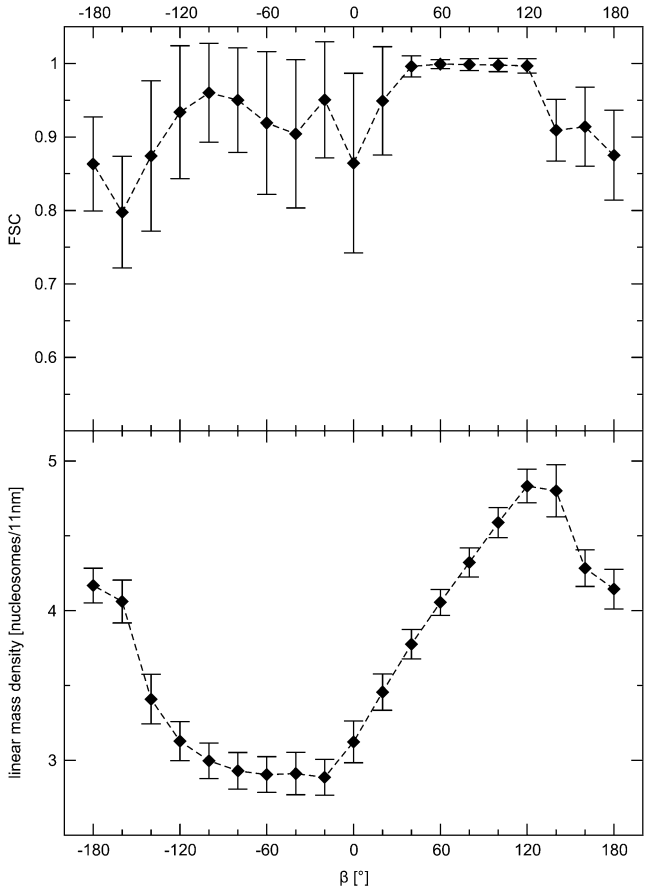

FIGURE 4 FSC and linear mass density as a function of the nucleosome twist angle β. The simulations were conducted with $\alpha = 26°$, NRL = 212 bp, and $E_{max} = 6\ kT$. The error bar indicates the standard deviation. The FSC indicated a plateau in the interval of 40–120° and for the linear mass density a peak at $\beta = 120°$.

Linker DNA length and twist angle affect the conformation of the chromatin fiber at thermal equilibrium

The influence of the linker DNA length on the fiber conformation was examined by varying the NRL value in 1 bp steps from 202 to 222 bp. To account for the helical twist of the DNA, the value of β was increased by 36° per basepair added to 212 bp and decreased by 36° per basepair for a shortening of the repeat length. The simulations were performed with E_{max} values of 1.5, 3, 6, 9, and 12 kT. Due to the large amount of computational time needed for simulations with $E_{max} > 6\ kT$, only three NRL values (206, 212, and 216 bp) were evaluated at these interaction strengths. The simulation results indicated peaks for the linear mass density and the radius of gyration at distances of ~10 bp (Fig. 5). For the linear mass density, a

TABLE 4 Results of Gaussian distributed nucleosome twist angles

E_{max} (kT)	1σ width of β-distribution (°)	Persistence length (nm)	FSC	PCA ratio	Linear mass density (nucleosomes/11 nm fiber)	Number of interdigitated nucleosomes	Radius of gyration (nm)
1.5	0	87.5 ± 4.1	$1 \pm 1.8 \times 10^{-3}$	5.38 ± 1.31	4.09 ± 0.11	0 ± 0	62.66 ± 6.9
1.5	10	83.1 ± 8.1	$1 \pm 1.8 \times 10^{-3}$	5.39 ± 1.31	4.09 ± 0.11	0 ± 0	62.62 ± 6.9
1.5	20	77.4 ± 8.7	$1 \pm 2.1 \times 10^{-3}$	5.35 ± 1.34	4.07 ± 0.11	0 ± 0	62.58 ± 7.18
1.5	30	66.5 ± 11	$1 \pm 3.3 \times 10^{-3}$	5.05 ± 1.37	4.06 ± 0.11	0 ± 0	60.98 ± 7.51
3	0	75.1 ± 8.2	$1 \pm 2.4 \times 10^{-3}$	5.22 ± 1.26	4.23 ± 0.11	0 ± 0	60.45 ± 6.77
3	10	76.6 ± 15.8	$1 \pm 2.0 \times 10^{-3}$	5.21 ± 1.28	4.22 ± 0.11	0 ± 0	60.39 ± 6.93
3	20	76.4 ± 14.4	$1 \pm 1.8 \times 10^{-3}$	5.10 ± 1.30	4.19 ± 0.11	0 ± 0	60.13 ± 7.16
3	30	53.8 ± 8	$1 \pm 1.8 \times 10^{-3}$	4.90 ± 1.29	4.19 ± 0.11	0 ± 0	58.91 ± 7.24
6	0	97.8 ± 11.1	$1 \pm 7.0 \times 10^{-3}$	5.21 ± 1.20	4.59 ± 0.10	$5.6 \times 10^{-3} \pm 7.5 \times 10^{-2}$	56.82 ± 6.99
6	10	78.4 ± 14.6	$1 \pm 5.0 \times 10^{-3}$	5.15 ± 1.16	4.59 ± 0.10	$2.1 \times 10^{-3} \pm 4.6 \times 10^{-2}$	56.74 ± 6.67
6	20	76.5 ± 12.4	$1 \pm 1.0 \times 10^{-2}$	5.00 ± 1.29	4.57 ± 0.11	$4.9 \times 10^{-3} \pm 7.9 \times 10^{-2}$	55.72 ± 7.45
6	30	65.9 ± 18.8	$0.98 \pm 3.1 \times 10^{-2}$	4.06 ± 1.43	4.59 ± 0.12	$1.9 \times 10^{-2} \pm 0.14$	49.00 ± 9.83

maximum at an NRL of 211 bp and a minima at 206 and 216 bp were found. For E_{max} values of 1.5 and 3 kT, the FSC value (~1) and the numbers of interdigitated nucleosomes (~0) were independent of the NRL. Chains simulated with $E_{max} \geq 6\ kT$ yielded higher variations of the FSC value, the radius of gyration, and the numbers of interdigitated nucleosomes (Fig. 5).

Depending on the nucleosome repeat length, different types of fiber typologies occurred, which were all in a crossed-linker DNA conformation (Fig. 6; supplementary VRML files, Data S2). The characteristics of these structures were pronounced at $E_{max} \geq 6\ kT$. Visual inspection of the trajectories revealed the formation of a right-handed three-start helix at NRL values of 202 and 212 bp (Fig. 6; Data S2; not all NRLs shown). At NRLs where the linear mass density achieved minima, a left-handed two-start helix with little twist (''parallel ribbon'') was detected. At NRLs >214 bp, the fibers were more irregular and adopted two-start helix structures.

The strength of the nucleosome-nucleosome interaction directs fiber compaction, fiber conformation, and higher order folding

Observation of the linear mass density in dependence on the internucleosomal interaction strength for an NRL of 212 bp indicated that the linear mass density increased continuously with E_{max} (Fig. 7). The decrease of the radius of gyration was indicative of a higher order folding of the chromatin fiber for $E_{max} > 6\ kT$. The 3D visualizations supported this conclusion, since chains with $E_{max} \leq 6\ kT$ folded into fibers, whereas chains with $E_{max} > 6\ kT$ folded also into hairpins or more compacted structures (Fig. 6; Data S2). At an NRL of 206 bp, a two-start zig-zag ribbon conformation was adopted, which displayed much less interwinding of the two stacks of nucleosomes than the other fibers (Fig. 6; Data S2). At $E_{max} = 9\ kT$, this fiber conformation exhibited self-associations of nucleosome arrays like hairpins and multiple folded arrays, both with interdigitated nucleosomes, and at $E_{max} = 12\ kT$ multiple folded and helical wrapped arrays were observed (Fig. 6; Data S2). For NRL = 216 bp and $E_{max} > 6\ kT$, structures with self-associated nucleosome arrays formed, which were characterized by interdigitated nucleosomes.

DISCUSSION

Due to its important function in controlling DNA accessibility for molecular biological processes, the theoretical description of the chromatin fiber organization has been the subject of a number of studies (11,12,15,16,18,22,26,27,46,66–69). In this work, the influence of the shape and strength of the nucleosome-nucleosome interaction potential on the folding of chains of 100 nucleosomes into a chromatin fiber was investigated at thermal equilibrium. To evaluate simulations over a broad range of interaction energies, a replica exchange protocol was developed, which improved the sampling of chromatin fibers in the MC simulations considerably. A local nucleosome geometry was examined that reproduced features of chromatin isolated from chicken erythrocytes. The ability of the chain to compact into a chromatin fiber was assessed by computing the linear mass density and its shape. The latter was quantitated by calculating FSC, PCA, and by computing the radius of gyration. Fiber-shaped structures were characterized by FSC values ≥0.9, a PCA ratio of longest/shortest axis >3, and a radius of gyration >45 nm (Figs. 4–6; Figs. S2 and S3, Data S2).

The influence of the nucleosome-nucleosome interaction potential on the conformation of the chromatin fiber

In the MC simulations, different nucleosome-nucleosome interaction potentials corresponding to different nucleosome shapes (spheres, ellipsoids, and spherocylinders) were compared. Spherical-shaped nucleosomes resulted in fiber struc-

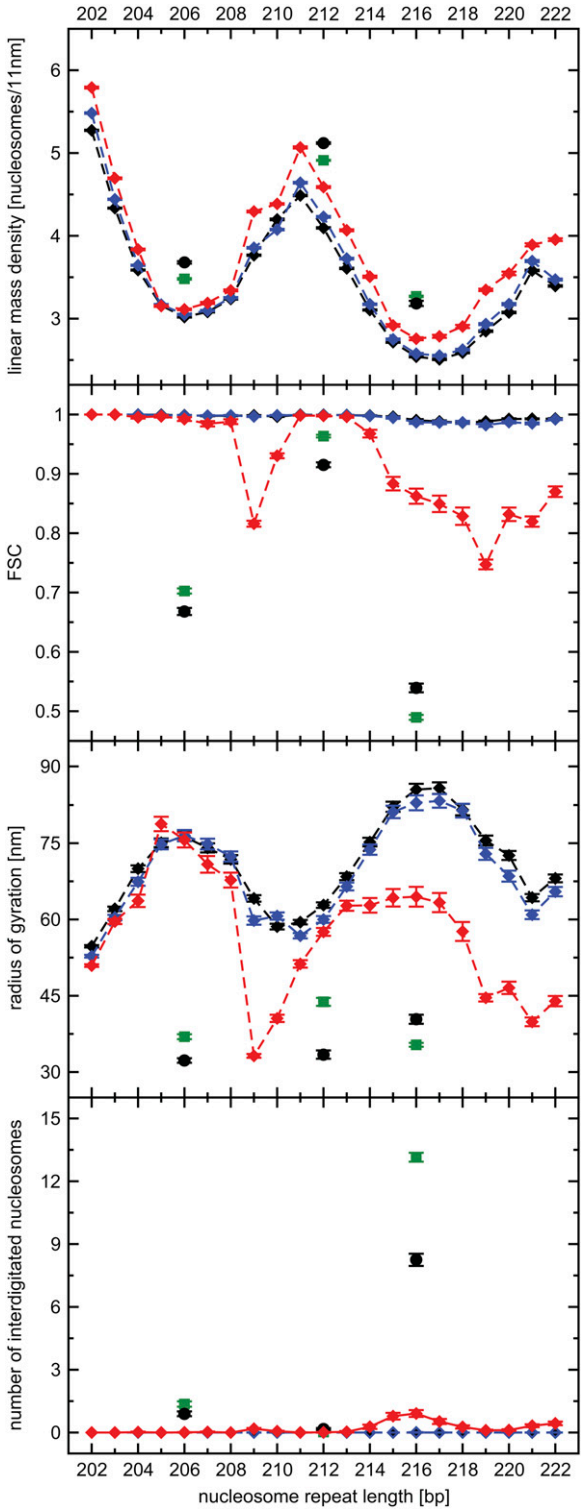

FIGURE 5 Linear mass density, FSC value, radius of gyration, and number of interdigitated nucleosomes as functions of the NRL for E_{max} of 1.5 (*black diamond*), 3 (*blue diamond*), 6 (*red diamond*), 9 (*green square*), and 12 *kT* (*black circle*). Error bars indicate the 95% confidence interval of the mean values. The model determined for chromatin from chicken erythrocytes ($\alpha = 26°$, $\beta = 100°$, and NRL = 212 bp) was investigated for NRLs varied in one basepair intervals. The value of β was increased by 36° for each basepair added and decreased by 36° for each basepair removed. The linear mass density and the radius of gyration yielded maxima in ~10 bp periodicity for all E_{max} values. For $E_{max} \leq 3$ *kT*, the FSC value and the number of interdigitated nucleosomes were independent of the NRL. Higher E_{max} values indicated crucial changing of all parameters but the linear mass density, which increased slightly with E_{max}.

tures for $E_{max} \leq 0.5$ *kT* (data not shown) and blob-like aggregates at higher interaction strength (Fig. 2), in agreement with previous simulations by Katritch et al. (15). In that study, similar compact irregular structures were found at interaction strengths >1 *kT*. Chains with ellipsoidal-shaped nucleosomes adopted stable fiber structures for E_{max} up to 1.5 *kT* (Fig. 2). The stability of these fibers was strongly dependent on the length of the linker DNA (Table 3), which is in agreement with previous results (22). Mergell et al. used ellipsoidal-shaped nucleosomes in the simulation of stretching single chromatin fibers and observed more compact structures like hairpins for nucleosome interaction strengths of up to 4 *kT* (18), in good agreement with the results reported here (Fig. 2).

Spherocylindrical-shaped nucleosomes led to stable fiber structures for E_{max} up to 6 *kT* and higher (Figs. 2 and 6). Recent investigations of the effective interaction energy of stacked nucleosomes indicated that the experimental measured interaction strength of 3.4 *kT* (31) was obtained with $E_{max} = 6$ *kT* (16). In the context of the chromatin fiber, other (energetically unfavorable) terms like DNA bending and electrostatic repulsion counteract the formation of nucleosome arrangements, in which the E_{max} value is reached. It is concluded that for the potentials and geometries investigated here, only the potential describing spherocylindrical-shaped nucleosomes is compatible with the formation of fiber-like chromatin structures in the regime of effective interaction energies of >2 *kT* that is physiologically the most relevant. This becomes even more important if one considers a potential stabilization of the nucleosome stacking due to a saturating linker histone content (19,32) or binding of additional chromosomal proteins (37–40,70) so that values of up to 10–16 *kT* might be reached, as discussed above.

Recently, cylindrical nucleosome descriptions have also been used for computer simulations of chromatin fibers as well as investigations of phase diagrams by analytical approaches (26,69). In the study by Cinacchi et al. (69), the energetics of nucleosome-nucleosome interactions were also described with a Zewdie potential to study the folding of nucleosome chains. The results are in good agreement with experimental data of liquid crystals of nucleosome core particles and support a two-start helical organization of the fiber in the absence of linker histones in a conformation that is similar to that found in the tetranucleosome (20).

The coarse-grained description of the nucleosome developed by Schlick and co-workers uses a so-called surface-charge optimization model (DiSCO) (11,12,21). In this model, the cylindrical shape of the nucleosome is implicitly included via the spatial distribution of charges that were di-

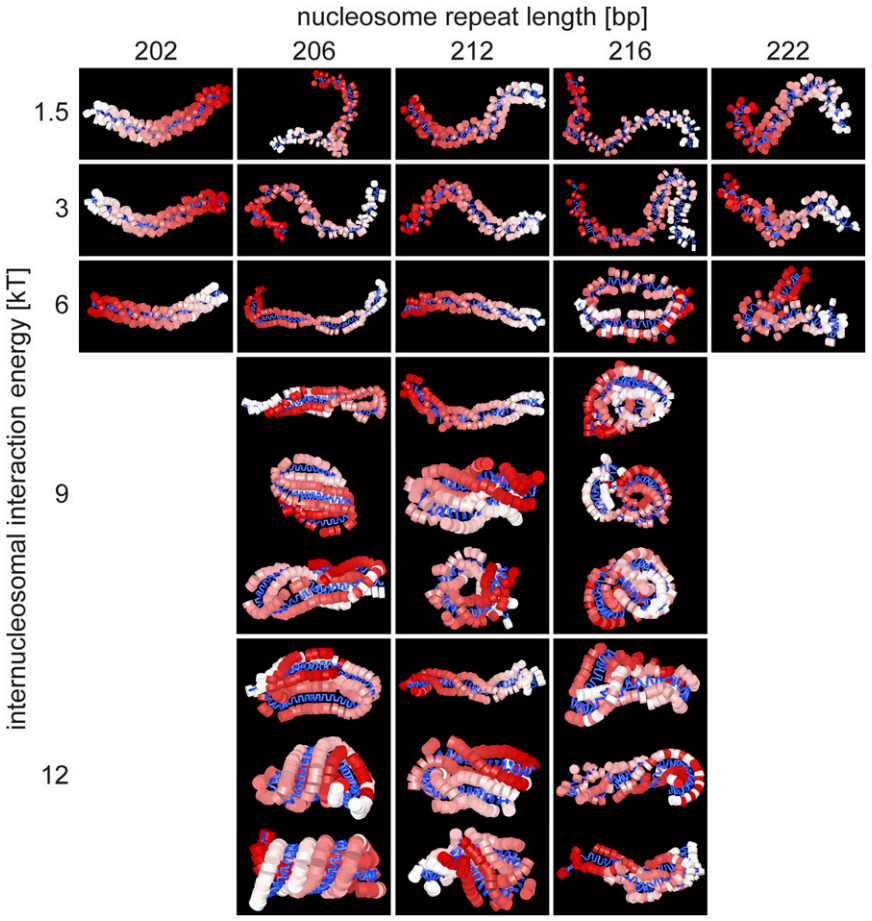

FIGURE 6 Visualization of simulated structures for E_{max} values between 1.5 and 12 kT. The nucleosomes are colored by their position in the chain (first is *white*, last is *red*) and the DNA segments are colored blue. The model determined for chromatin from chicken erythrocytes ($\alpha = 26°$, $\beta = 100°$, and NRL = 212 bp) was investigated for NRLs varied in one basepair intervals. The value of β was increased by 36° for each basepair added and decreased by 36° for each basepair removed. At $E_{max} \geq 6\ kT$ with NRL values of 202 and 212 bp, a right-handed three-start helix conformation with crossed DNA linker occurred, whereas other NRLs led to a left-handed two-start helix (e.g., at the minima of the linear mass density). NRLs > 214 bp exhibited more irregular structures. Depending on the NRL and E_{max}, self association of distant fiber parts was apparent. Systems with an NRL of 212 bp and $E_{max} > 6\ kT$ exhibited fiber structures, which were sometimes folded to hairpins, whereas for NRL = 206 bp, a ribbon-like structure folded back into several different superstructures with oval or helical backbone shapes. At NRL = 216 bp and in part at 206 bp, interdigitation of nucleosomes was apparent with several kinds of structures. For 3D visualization of the fiber, see the supplementary VRML files (Data S2).

rectly derived from the nucleosome crystal structure. The DiSCO model has been applied successfully for investigations of the salt-dependent compaction of oligonucleosomes and the role of histone tails in mediating internucleosomal interactions (11,12,21). Visualizations of 12, 24, and 48 oligonucleosome arrays show somewhat more irregular fiber conformations than those observed in most of the trajectories evaluated here (11,21). The reasons for these differences remain to be elucidated but are likely to be related to the absence of linker histones in the simulations reported so far for the DiSCO model.

From the systematic analysis of the fiber stability conducted here, it can be concluded that the cylindrical shape of the nucleosome potential as well as the strength and orientation dependence of the interaction between nucleosomes are important parameters for controlling the folding of the chromatin fiber. The local nucleosome geometry studied here was chosen to fit experimental findings for chromatin fibers from chicken erythrocytes with 212 bp NRL. For this conformation, two- and three-start helices with crossed-linker DNA were found to be most favorable up to $E_{max} = 6\ kT$, whereas at higher interaction energies other conformations were present (Fig. 6; Figs. S2 and S4, Data S1).

Features of chicken erythrocyte chromatin fibers inferred from the MC simulations

The twist angle between consecutive nucleosomes cannot be directly retrieved from the experimental analysis of chro-

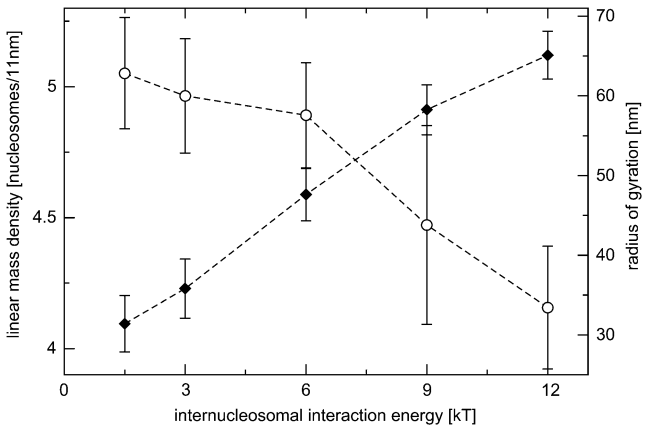

FIGURE 7 Linear mass density (♦) and the radius of gyration (○) as functions of E_{max}. The simulations were conducted for the model determined for chromatin from chicken erythrocytes ($\alpha = 26°$, $\beta = 100°$, and NRL = 212 bp). Error bars indicate the standard deviation. The linear mass density increased nearly linear with E_{max}, whereas the radius of gyration exhibited an abrupt change between E_{max} values of 6 and 9 kT.

matin fibers from chicken erythrocytes, in contrast to the value of the entry-exit angle α (13). Accordingly, a range of β-values was studied in the simulations reported here (Fig. 4; Figs. S2 and S3, Data S1). A value of ~100° was found to yield a stable fiber conformation, in a good agreement with the experimental data as well as previous MC simulations (22,46). The linear mass density reached a maximum of ~5.1 nucleosomes/11 nm fiber for NRL = 212 bp with E_{max} = 12 kT (Fig. 7) and ~5.8 nucleosomes/11 nm fiber for NRL = 202 bp with E_{max} = 6 kT (Fig. 5). This is close to the experimentally determined value of 6–7 nucleosomes/11 nm fiber for chicken chromatin (13,41,42). At an NRL value of 212 bp, a fiber diameter of 30 nm was obtained (Fig. S5, Data S1), as measured for chromatin from chicken erythrocytes at physiological salt concentration in several studies (17,41, 42,63,71). Since the nucleosome repeat length of native chromatin is not exactly constant but varies by 1–3 basepairs (1), simulations of Gaussian distributed β-values were also performed. The results indicated that the overall fiber conformation changed only moderately but revealed a softening of the fiber, as apparent from a reduction of its persistence length (Table 4; Fig. S4, Data S1). This behavior is similar to previous results obtained at lower nucleosome-nucleosome interaction strength (22). The impact of local variations of the NRL was also addressed by Bešker et al. in investigations of the nucleosome packing energy for local variations of the NRL for bulk chromatin around the value of chromatin from chicken erythrocytes for different nucleosome geometries (68). It was found that the stem motif, which has been used in this work, is the most favorable and that conformations with nearly equal NRL values between adjacent nucleosome pairs yielded minima of the nucleosome stacking energy.

The persistence lengths determined here were between 50 and 100 nm for an NRL of 212 bp and different widths of the Gaussian nucleosome twist angle distribution centered around $\beta = 110°$ (Table 4). Previously, values of 49 nm (22) and 40–50 nm (46) were reported for similar fiber geometries and NRLs between 212 and 205 bp, respectively. The somewhat higher values derived here are likely to reflect differences in the shape and orientation dependence of the nucleosome interaction potential. The results of all three studies are well within the rather broad range of 30–220 nm determined experimentally for the chromatin fiber persistence lengths (72).

Simulations, in which the NRL and the corresponding twist angle β were varied, demonstrated the large effect of this parameter on the stability of the fiber and a ~10 bp periodicity (Fig. 5; Fig. S5, Data S1). The latter is consistent with NRLs found in natural sequences (73), the experimental analysis of chromatin fibers reconstituted in vitro (19), and previous MC simulations of other fiber types (16). For the fiber conformation studied here, mass density and fiber diameter changed continuously with the NRL at the maxima at 202, 212, and 222 bp (Fig. 5; Fig. S5, Data S1). This is in agreement with investigations of chromatin from different tissues by x-ray scattering and electron microscopy (74). In contrast, the results from Robinson et al. obtained with reconstituted chromatin fibers revealed a nearly constant fiber mass density and diameter below an NRL of 207 bp with a transition between 207 and 217 bp to a fiber structure with higher mass density and diameter (19). Thus, the compatibility with certain NRLs appears to be a characteristic feature of different fiber types. It might also be a crucial parameter to induce transitions between different fiber conformations. This is evident from the simulations conducted here. Chains with NRL values of 202 and 212 bp yielded a right-handed three-start helix with crossed-linker DNA (Fig. 6; Data S2). Upon changing the nucleosome repeat length, the three-start helix transformed into a two-start helix with a zig-zag ribbon motif, which has also been found in experimental studies of native chromatin from chicken erythrocytes (13,63,71,75) and by computer simulations of chromatin (69). It remains to be examined in further detail if the observed three-start helix conformation at NRL = 212 bp would be compatible with electron microscopy data like, for example, those reported by Dorigo et al., for which a two-start zig-zag ribbon motif has been proposed (64).

NRL values >214 bp were found to yield more irregular structures (Figs. 5 and 6). This effect can be explained by higher electrostatic repulsion of longer linker DNA (76) and its larger flexibility, and is similar to recent results from MC simulations of different chromatin models (16). As concluded by Kobori et al. from atomic force microscopy investigations of chromatin unfolding processes, longer linker requires the binding of linker histones to form higher-order chromatin (76). This is in agreement with results from MC simulations of the tetranucleosome structure without linker histone, which exhibited more irregular structures by increasing the linker length. If linker histones are present, fiber structures for NRLs up to 214 bp can be found (Figs. 5 and 6).

Experimental studies have revealed breaks in the zig-zag-like backbone of chicken chromatin fibers (63), with the ribbon-like conformation in some cases being restricted to short parts of the fiber, whereas other regions appeared to be rather irregular (17,71). Based on topological models of chromatin fibers, this was explained by NRL variations between consecutive nucleosomes (24,71). The results obtained here suggest that these structural changes could also result from differences in the strength of internucleosomal interaction in certain parts of the native fibers. Recently, all-atom structures were reported for fibers with NRLs from 177 to 237 bp in a 2–5 start-helix conformation and with varying handedness (23). In the latter study, a transition from left- or right-handed three-start helix structures to right-handed two-start helix structures was described that was induced by increasing the NRL from 197 to 207. Furthermore, one-, two-, and three-start-helix conformations were found for different combinations of the entry-exit-angle, twist-angle, and linker length by MC simulations (69). Our results support the view

that such a transition would not only be compatible with the topological constraints of the nucleosome chain, but could also be energetically favorable.

The impact of the internucleosomal interaction strength on the compaction and higher order folding of chromatin

The simulated fibers with NRLs $<$ 214 bp exhibited a relatively tight nucleosome stacking (Fig. 6; Data S2) consistent with a number of experimental and modeling studies (16,19,20,23). However, in the experimental analysis of chromatin from chicken erythrocytes in vivo and in situ by various imaging-based approaches, the conformational variability of this parameter seems to be significant (13,44, 63,71). In some of the structures, the nucleosome chain appeared relatively open with distances between neighboring nucleosomes that appeared to be larger than those found in the tetranucleosome crystal structure, which is likely to represent a bona fide energetically favorable arrangement of two nucleosomes in close contact (20). For a fixed β-value, the linear mass density increased linearly with E_{max} up to ~5.1 and ~5.8 nucleosomes/11 nm fiber for NRL values of 212 and 202 bp, respectively (Figs. 5 and 7). Since any increase of the distance between nucleosomes is likely to further reduce the fiber mass density, it is concluded that the degree of nucleosome stacking observed in the simulations is required to reach the compaction of the chromatin fiber observed under physiological conditions (13,41,42). Recent investigations of reconstituted nucleosome arrays yielded surprisingly high mass densities of ~12–~15 nucleosomes/11 nm fiber (19). From inspection of the electron microscopy images of these structures, their folding appears to be different from that of native chicken chromatin fiber fragments (13,44,63,71).

The abrupt change of the radius of gyration and the FSC value at E_{max} between 6 and 9 kT (Figs. 5 and 7) are indicative of a higher order folding of the chromatin fiber. Self-association of chromatin fibers has been reported to increase the apparent fiber diameter from ~45 nm up to 100–200 nm as reviewed recently by Horn (77) and Grigoryev (78). In the MC simulations, different types of self associations were observed depending on the fiber topology (Fig. 6; Data S2). The three-start helix at NRL = 212 bp persisted in most cases as a fiber structure and folded back into hairpins, whereas the structures at NRL = 206 bp yielded complex folds with oval or helical backbone shapes. From experimental data, it is known that the higher order folding of chromatin is controlled by the linker histone and the so-called chromatin architectural proteins, like for example the linker histone, HP1, and MeCP2 (37,38). As described above for HP1, these proteins are likely to increase the internucleosomal interaction strength considerably so that values are reached that are similar in magnitude to the higher E_{max} values used here. In addition, the salt dependence of the chromatin fiber compaction as well as the effect of posttranslational histone modifications support the view that the nucleosome interaction strength can be modulated over a rather broad range.

Interestingly, fibers with NRLs of 206 and 216 bp exhibited interdigitation of nucleosomes (Figs. 5 and 6; Data S2). A similar result was obtained for variation of β in the interval from −80° to 20° (Fig. S3, Data S1), where interdigitated nucleosomes were often found at the start and endpoint of chromatin loops. Experimental evidence for interdigitated nucleosome arrangements is based on in situ studies of chicken erythrocytes (71), investigations of heterochromatin (see Grigoryev (78) and references therein), and the electron microscopy analysis of reconstituted chromatin fibers (19).

CONCLUSION

Chromatin represents a highly complex supramolecular system that can adopt a variety of conformational states depending on its constituting components. The use of MC simulations is ideally suited to evaluate its differential organization in thermal equilibrium by taking advantage of our detailed and increasing knowledge of the nucleosome as the building block of the chromatin fiber. Here, the effect of the shape and the strength of the nucleosome-nucleosome interaction potential was evaluated, whereas in the companion article in this issue, the effect of different local nucleosome geometries was investigated in further detail (16). Taken together, these two studies link distinct local nucleosome properties to strikingly different fiber conformations that have been observed in experimental studies (13,19,20). In vivo, transitions between these fiber structures could be induced by the binding of linker histones or other chromosomal proteins (HP1, MeCP2, HMGN, etc.) or by posttranslational modification of core histones. The formation of various fiber conformations is likely to translate also into differences in the higher-order folding of chromatin fibers on the length scale of 0.1–1 Mb of DNA, for which various models have been proposed (79,80). Interestingly, the simulations conducted here with chains of 100 nucleosomes (~20 kb DNA) revealed some differences in the folding of the fiber that become apparent at higher nucleosome-nucleosome interaction strength. To extract more detailed information about the interactions among different domains of the nucleosome chain, it is planned to extend the MC simulations to the length scale of 500–1000 nucleosomes (or 100–200 kb DNA). These fibers are significantly longer than the persistence length of the fiber, and it is anticipated that a comparison of different fiber types will lead to further insight into the factors that govern the higher order folding of the chromatin fiber.

SUPPLEMENTARY MATERIAL

To view all of the supplemental files associated with this article, visit www.biophysj.org.

We are grateful to Sören Wolter for writing the chromatin visualization tool and to Reyk Weiss for performance optimization of the simulation software, writing the VRLM export and assistance with the simulations at the HLRN. Furthermore, we thank Dr. Helmut Katzgraber for valuable discussions on replica exchange simulations and Ramona Ettig for critical reading of the manuscript.

This work was supported by the Volkswagen Foundation in the programs ''New Conceptual Approaches to Modeling and Simulation of Complex Systems'' and ''Junior Research Groups at German Universities'' and by the University of Applied Sciences Stralsund (HWP11042401). Most of the computations were done on the IBM pSeries 690 Supercomputer of the HLRN, Berlin/Hannover (mvb00007).

REFERENCES

1. van Holde, K. E. 1989. Chromatin. Springer, Heidelberg.
2. Woodcock, C. L., and S. Dimitrov. 2001. Higher-order structure of chromatin and chromosomes. *Curr. Opin. Genet. Dev.* 11:130–135.
3. Luger, K., and J. C. Hansen. 2005. Nucleosome and chromatin fiber dynamics. *Curr. Opin. Struct. Biol.* 15:188–196.
4. Robinson, P. J., and D. Rhodes. 2006. Structure of the '30 nm' chromatin fibre: a key role for the linker histone. *Curr. Opin. Struct. Biol.* 16:336–343.
5. Tremethick, D. J. 2007. Higher-order structures of chromatin: the elusive 30 nm fiber. *Cell.* 128:651–654.
6. Luger, K., A. W. Mäder, R. K. Richmond, D. F. Sargent, and T. J. Richmond. 1997. Crystal structure of the nucleosome core particle at 2.8 Å resolution. *Nature.* 389:251–260.
7. Davey, C. A., D. F. Sargent, K. Luger, A. W. Maeder, and T. J. Richmond. 2002. Solvent mediated interactions in the structure of the nucleosome core particle at 1.9 Å resolution. *J. Mol. Biol.* 319:1097–1113.
8. Fan, Y., T. Nikitina, J. Zhao, T. J. Fleury, R. Bhattacharyya, E. E. Bouhassira, A. Stein, C. L. Woodcock, and A. I. Skoultchi. 2005. Histone H1 depletion in mammals alters global chromatin structure but causes specific changes in gene regulation. *Cell.* 123:1199–1212.
9. Widom, J., and A. Klug. 1985. Structure of the 300A chromatin filament: X-ray diffraction from oriented samples. *Cell.* 43:207–213.
10. Finch, J. T., and A. Klug. 1976. Solenoidal model for superstructure in chromatin. *Proc. Natl. Acad. Sci. USA.* 73:1897–1901.
11. Arya, G., and T. Schlick. 2006. Role of histone tails in chromatin folding revealed by a mesoscopic oligonucleosome model. *Proc. Natl. Acad. Sci. USA.* 103:16236–16241.
12. Beard, D. A., and T. Schlick. 2001. Computational modeling predicts the structure and dynamics of chromatin fiber. *Structure.* 9:105–114.
13. Bednar, J., R. A. Horowitz, S. A. Grigoryev, L. M. Carruthers, J. C. Hansen, A. J. Koster, and C. L. Woodcock. 1998. Nucleosomes, linker DNA, and linker histone form a unique structural motif that directs the higher-order folding and compaction of chromatin. *Proc. Natl. Acad. Sci. USA.* 95:14173–14178.
14. Daban, J. R., and A. Bermudez. 1998. Interdigitated solenoid model for compact chromatin fibers. *Biochemistry.* 37:4299–4304.
15. Katritch, V., C. Bustamante, and W. K. Olson. 2000. Pulling chromatin fibers: computer simulations of direct physical micromanipulations. *J. Mol. Biol.* 295:29–40.
16. Kepper, N., D. Foethke, R. Stehr, G. Wedemann, and K. Rippe. 2008. Nucleosome geometry and internucleosomal interactions control the chromatin fiber conformation. *Biophys. J.* 95:3692–3705.
17. Leuba, S. H., G. Yang, C. Robert, B. Samori, K. van Holde, J. Zlatanova, and C. Bustamante. 1994. Three-dimensional structure of extended chromatin fibers as revealed by tapping-mode scanning force microscopy. *Proc. Natl. Acad. Sci. USA.* 91:11621–11625.
18. Mergell, B., R. Everaers, and H. Schiessel. 2004. Nucleosome interactions in chromatin: Fiber stiffening and hairpin formation. *Phys. Rev. E.* 70:011915.
19. Robinson, P. J., L. Fairall, V. A. Huynh, and D. Rhodes. 2006. EM measurements define the dimensions of the ''30-nm'' chromatin fiber: evidence for a compact, interdigitated structure. *Proc. Natl. Acad. Sci. USA.* 103:6506–6511.
20. Schalch, T., S. Duda, D. F. Sargent, and T. J. Richmond. 2005. X-ray structure of a tetranucleosome and its implications for the chromatin fibre. *Nature.* 436:138–141.
21. Sun, J., Q. Zhang, and T. Schlick. 2005. Electrostatic mechanism of nucleosomal array folding revealed by computer simulation. *Proc. Natl. Acad. Sci. USA.* 102:8180–8185.
22. Wedemann, G., and J. Langowski. 2002. Computer simulation of the 30-nanometer chromatin fiber. *Biophys. J.* 82:2847–2859.
23. Wong, H., J.-M. Victor, and J. Mozziconacci. 2007. An all-atom model of the chromatin fiber containing linker histones reveals a versatile structure tuned by the nucleosomal repeat length. *PLoS ONE.* 2:e877.
24. Woodcock, C. L., S. A. Grigoryev, R. A. Horowitz, and N. Whitaker. 1993. A chromatin folding model that incorporates linker variability generates fibers resembling the native structures. *Proc. Natl. Acad. Sci. USA.* 90:9021–9025.
25. Wu, C., A. Bassett, and A. Travers. 2007. A variable topology for the 30-nm chromatin fibre. *EMBO Rep.* 8:1129–1134.
26. Diesinger, P. M., and D. W. Heermann. 2008. The influence of the cylindrical shape of the nucleosomes and H1 defects on properties of chromatin. *Biophys. J.* 94:4165–4172.
27. Schiessel, H., W. M. Gelbart, and R. Bruinsma. 2001. DNA folding: structural and mechanical properties of the two- angle model for chromatin. *Biophys. J.* 80:1940–1956.
28. Widom, J. 1989. Toward a unified model of chromatin folding. *Annu. Rev. Biophys. Biophys. Chem.* 18:365–395.
29. van Holde, K., and J. Zlatanova. 1996. What determines the folding of the chromatin fiber. *Proc. Natl. Acad. Sci. USA.* 93:10548–10555.
30. Hamiche, A., P. Schultz, V. Ramakrishnan, P. Oudet, and A. Prunell. 1996. Linker histone-dependent DNA structure in linear mononucleosomes. *J. Mol. Biol.* 257:30–42.
31. Cui, Y., and C. Bustamante. 2000. Pulling a single chromatin fiber reveals the forces that maintain its higher-order structure. *Proc. Natl. Acad. Sci. USA.* 97:127–132.
32. Kruithof, M., F. Chien, M. de Jager, and J. van Noort. 2008. Subpiconewton dynamic force spectroscopy using magnetic tweezers. *Biophys. J.* 94:2343–2348.
33. Draves, P. H., P. T. Lowary, and J. Widom. 1992. Co-operative binding of the globular domain of histone H5 to DNA. *J. Mol. Biol.* 225:1105–1121.
34. Thomas, J. O., C. Rees, and J. T. Finch. 1992. Cooperative binding of the globular domains of histones H1 and H5 to DNA. *Nucleic Acids Res.* 20:187–194.
35. Solis, F. J., R. Bash, J. Yodh, S. M. Lindsay, and D. Lohr. 2004. A statistical thermodynamic model applied to experimental AFM population and location data is able to quantify DNA-histone binding strength and internucleosomal interaction differences between acetylated and unacetylated nucleosomal arrays. *Biophys. J.* 87:3372–3387.
36. Shogren-Knaak, M., H. Ishii, J.-M. Sun, M. J. Pazin, J. R. Davie, and C. L. Peterson. 2006. Histone H4–K16 acetylation controls chromatin structure and protein interactions. *Science.* 311:844–847.
37. McBryant, S., V. Adams, and J. Hansen. 2006. Chromatin architectural proteins. *Chromosome Res.* 14:39–51.
38. Woodcock, C. L. 2006. Chromatin architecture. *Curr. Opin. Struct. Biol.* 16:213–220.
39. Maison, C., and G. Almouzni. 2004. HP1 and the dynamics of heterochromatin maintenance. *Nat. Rev. Mol. Cell Biol.* 5:296–304.
40. Zhao, T., T. Heyduk, C. D. Allis, and J. C. Eissenberg. 2000. Heterochromatin protein 1 binds to nucleosomes and DNA in vitro. *J. Biol. Chem.* 275:28332–28338.
41. Gerchman, S. E., and V. Ramakrishnan. 1987. Chromatin higher-order structure studied by neutron scattering and scanning transmission electron microscopy. *Proc. Natl. Acad. Sci. USA.* 84:7802–7806.

42. Ghirlando, R., and G. Felsenfeld. 2008. Hydrodynamic studies on defined heterochromatin fragments support a 30-nm fiber having six nucleosomes per turn. *J. Mol. Biol.* 376:1417–1425.
43. Hansen, J. C., J. Ausio, V. H. Stanik, and K. E. van Holde. 1989. Homogeneous reconstituted oligonucleosomes, evidence for salt-dependent folding in the absence of histone H1. *Biochemistry.* 28:9129–9136.
44. Bednar, J., R. A. Horowitz, J. Dubochet, and C. L. Woodcock. 1995. Chromatin conformation and salt-induced compaction: three-dimensional structural information from cryoelectron microscopy. *J. Cell Biol.* 131:1365–1376.
45. Mangenot, S., A. Leforestier, P. Vachette, D. Durand, and F. Livolant. 2002. Salt-induced conformation and interaction changes of nucleosome core particles. *Biophys. J.* 82:345–356.
46. Aumann, F., F. Lankas, M. Caudron, and J. Langowski. 2006. Monte Carlo simulation of chromatin stretching. *Phys. Rev.* 73:041927.
47. Ehrlich, L., C. Munkel, G. Chirico, and J. Langowski. 1997. A Brownian dynamics model for the chromatin fiber. *Comput. Appl. Biosci.* 13:271–279.
48. Stone, A. J. 1978. The description of bimolecular potentials, forces and torques: the S and V function expansions. *Mol. Phys.* 36:241–256.
49. Zewdie, H. 1998. Computer-simulation studies of diskotic liquid crystals. *Phys. Rev. E.* 57:1793–1805.
50. Metropolis, N., A. Rosenbluth, M. Roenbluth, A. Teller, and E. Teller. 1953. Equation of state calculations by fast computing machines. *J. Chem. Phys.* 21:1087–1092.
51. Baumgärtner, A., and K. Binder. 1979. Monte Carlo studies on the freely jointed polymer chain with excluded volume interaction. *J. Chem. Phys.* 71:2541–2545.
52. Freire, J. J., and A. Horta. 1976. Mean reciprocal distances of short polymethylene chains. Calculation of the translational diffusion coefficient of *n*-alkanes. *J. Chem. Phys.* 65:4049–4054.
53. Swendsen, R. H., and J.-S. Wang. 1986. Replica Monte Carlo simulation of spin-glasses. *Phys. Rev. Lett.* 57:2607–2609.
54. Hansmann, U. H. E. 1997. Parallel tempering algorithm for conformational studies of biological molecules. *J. Stat. Phys.* 281:140–150.
55. Hukushima, K., and K. Nemoto. 1996. Exchange Monte Carlo method and application to spin glass simulations. *J. Phys. Soc. Jpn.* 65:1604–1608.
56. Schug, A., T. Herges, A. Verma, and W.Wenzel. 2005. Investigation of the parallel tempering method for protein folding. *J. Phys. Condens. Matter.* 17:1641–1650.
57. Sugita, Y., and Y. Okamoto. 1999. Replica-exchange molecular dynamics method for protein folding. *Chem. Phys. Lett.* 314:141–151.
58. Katzgraber, H. G., S. Trebst, D. A. Huse, and M. Troyer. 2006. Feedback-optimized parallel tempering Monte Carlo. *J. Stat. Mech. Theor. Exp.* P03018:03018.
59. Rathore, N., M. Chopra, and J. J. de Pablo. 2005. Optimal allocation of replicas in parallel tempering simulations. *J. Chem. Phys.* 122:024111.
60. Kirkpatrick, S., C. D. Gelatt Jr., and M. P. Vecchi. 1983. Optimization by simulated annealing. *Science.* 220:671–680.
61. Bloomfield, V. A., D. M. Crothers, and I. Tinocco. 2000. Nucleic Acids: Structures, Properties, and Functions. University Science Books, Sausalito, CA.
62. Livolant, F., S. Mangenot, A. Leforestier, A. Bertin, M. Frutos, E. Raspaud, and D. Durand. 2006. Are liquid crystalline properties of nucleosomes involved in chromosome structure and dynamics? *Philos. Trans. R. Soc. A.* 364:2615–2633.
63. Woodcock, C., L. Frado, and J. Rattner. 1984. The higher-order structure of chromatin: evidence for a helical ribbon arrangement. *J. Cell Biol.* 99:42–52.
64. Dorigo, B., T. Schalch, A. Kulangara, S. Duda, R. R. Schroeder, and T. J. Richmond. 2004. Nucleosome arrays reveal the two-start organization of the chromatin fiber. *Science.* 306:1571–1573.
65. Yodh, J. G., N. Woodbury, L. S. Shlyakhtenko, Y. L. Lyubchenko, and D. Lohr. 2002. Mapping nucleosome locations on the 208–12 by AFM Provides clear evidence for cooperativity in array occupation. *Biochemistry.* 41:3565–3574.
66. Muhlbacher, F., C. Holm, and H. Schiessel. 2006. Controlled DNA compaction within chromatin: the tail-bridging effect. *Europhys. Lett.* 73:135–141.
67. Muhlbacher, F., H. Schiessel, and C. Holm. 2006. Tail-induced attraction between nucleosome core particles. *Phys. Rev. E.* 74:031919.
68. Bešker, N., C. Anselmib, and P. D. Santis. 2004. Theoretical models of possible compact nucleosome structures. *Biophys. Chem.* 115:139–143.
69. Cinacchi, G., G. L. Penna, and A. Perico. 2007. Anisotropic internucleosome interactions and geometrical constraints in the organization of chromatin. *Macromolecules.* 40:9603–9613.
70. Woodcock, C. L., A. I. Skoultchi, and Y. Fan. 2006. Role of linker histone in chromatin structure and function: H1 stoichiometry and nucleosome repeat length. *Chromosome Res.* 14:17–25.
71. Horowitz, R. A., D. A. Agard, J. W. Sedat, and C. L. Woodcock. 1994. The three-dimensional architecture of chromatin in situ: electron tomography reveals fibers composed of a continuously variable zigzag nucleosomal ribbon. *J. Cell Biol.* 125:1–10.
72. Rippe, K. 2001. Making contacts on a nucleic acid polymer. *Trends Biochem. Sci.* 26:733–740.
73. Widom, J. 1992. A relationship between the helical twist of DNA and the ordered positioning of nucleosomes in all eukaryotic cells. *Proc. Natl. Acad. Sci. USA.* 89:1095–1099.
74. Williams, S. P., B. D. Athey, L. J. Muglia, R. S. Schappe, A. H. Gough, and J. P. Langmore. 1986. Chromatin fibers are left-handed double helices with diameter and mass per unit length that depend on linker length. *Biophys. J.* 49:233–248.
75. Leuba, S. H., C. Bustamante, K. van Holde, and J. Zlatanova. 1998. Linker histone tails and N-tails of histone H3 are redundant: scanning force microscopy studies of reconstituted fibers. *Biophys. J.* 74:2830–2839.
76. Kobori, T., S. Iwamoto, K. Takeyasu, and T. Ohtani. 2007. Chromatin dynamics of unfolding and refolding controlled by the nucleosome repeat length and the linker and core histones. *Biopolymers.* 85:295–307.
77. Horn, P. J., and C. L. Peterson. 2002. Chromatin higher order folding: wrapping up transcription. *Science.* 297:1824–1827.
78. Grigoryev, S. A. 2004. Keeping fingers crossed: heterochromatin spreading through interdigitation of nucleosome arrays. *FEBS Lett.* 564:4–8.
79. Cremer, T., M. Cremer, S. Dietzel, S. Muller, I. Solovei, and S. Fakan. 2006. Chromosome territories—a functional nuclear landscape. *Curr. Opin. Cell Biol.* 18:307–316.
80. Rippe, K., J. Mazurkiewicz, and N. Kepper. 2008. Interactions of histones with DNA: nucleosome assembly, stability and dynamics. *In* DNA Interactions with Polymers and Surfactants. B. Lindman and R. Dias, editors. Wiley-Blackwell, London. 135–172.

SUPPLEMENTARY MATERIALS

The effect of the internucleosomal interaction on the folding of the chromatin fiber

René Stehr*, Nick Kepper†, Karsten Rippe†, Gero Wedemann*[1]

* University of Applied Sciences Stralsund, System Engineering and Information Management, Zur Schwedenschanze 15, 18435 Stralsund, Germany

† Deutsches Krebsforschungszentrum & BIOQUANT, Research Group Genome Organization & Function, Im Neuenheimer Feld 280, 69120 Heidelberg, Germany

[1] to whom correspondence should be addressed: gero.wedemann@fh-stralsund.de

SUPPLEMENTARY TABLES

TABLE S1: Parameters used in the MC simulations

Parameter	Value
Stretching module DNA	$1.10 \cdot 10^{-18}$ J nm
Bending module DNA	$2.06 \cdot 10^{-19}$ J nm
Torsion module DNA	$2.67 \cdot 10^{-19}$ J nm
Electrostatic radius DNA	1.2 nm
Stretching module chromatosome	$1.10 \cdot 10^{-18}$ J nm
Torsion module chromatosome	$1.30 \cdot 10^{-18}$ J nm
Temperature	293 K
Ionic strength	100 mM NaCl

SUPPLEMENTARY FIGURES

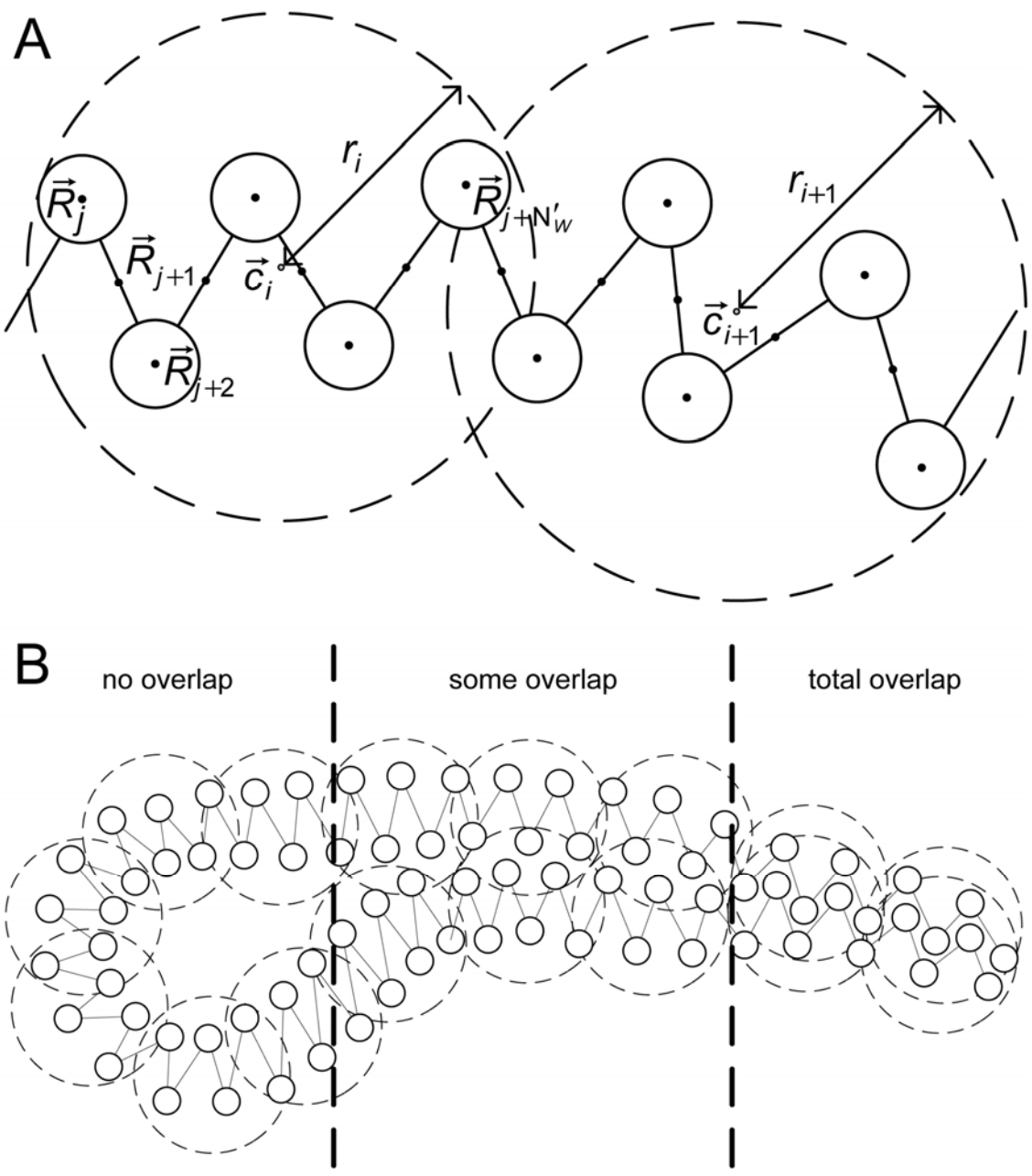

FIGURE S1. (A) The FSC algorithm approximates the shape of the chromatin fiber as a series of spheres. The center vector $\vec{c}_i$ corresponding to the sphere of the region i is defined as the mean of the center vectors $\vec{R}_i$ of the nucleosome and DNA beads. The radius r_i is the maximum distance between the center point $\vec{c}_i$ and all considered beads. A number of N_w beads was used for determining one sphere. (B) Schematic example of a folded chromatin fiber. For simplification, all shape-spheres have the same radius. The fiber is divided into three sections with no, some and total overlap of the spheres and approximate FSC values of 1, 0.7 and 0.5, respectively.

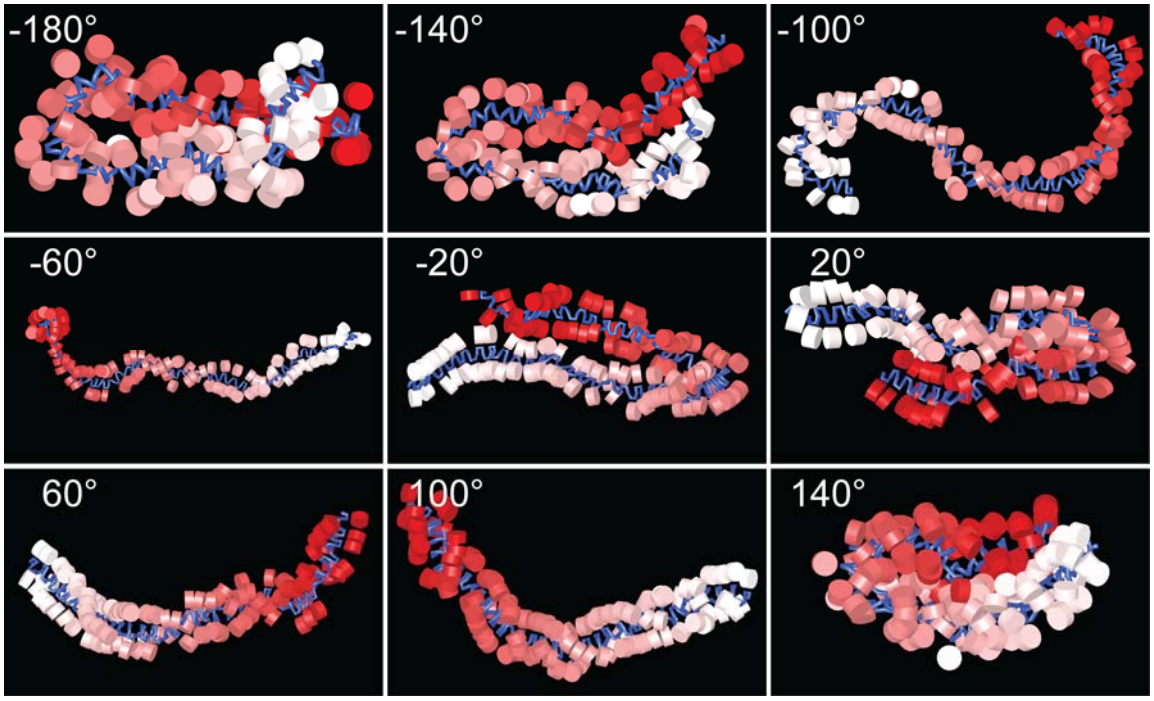

FIGURE S2. Variation of the twist angle β between consecutive nucleosomes from -180 – 180° for chicken erythrocyte chromatin. The nucleosomes are colored by their position in the chain (first is white, last is red) and the DNA segments are colored blue. The simulations were conducted with α = 26°, NRL = 212 bp and E_{max} = 6 kT. For β values in the interval of 40° – 120° (not all shown) fiber structures occurred. At β = 100° a right-handed three-start helix was apparent.

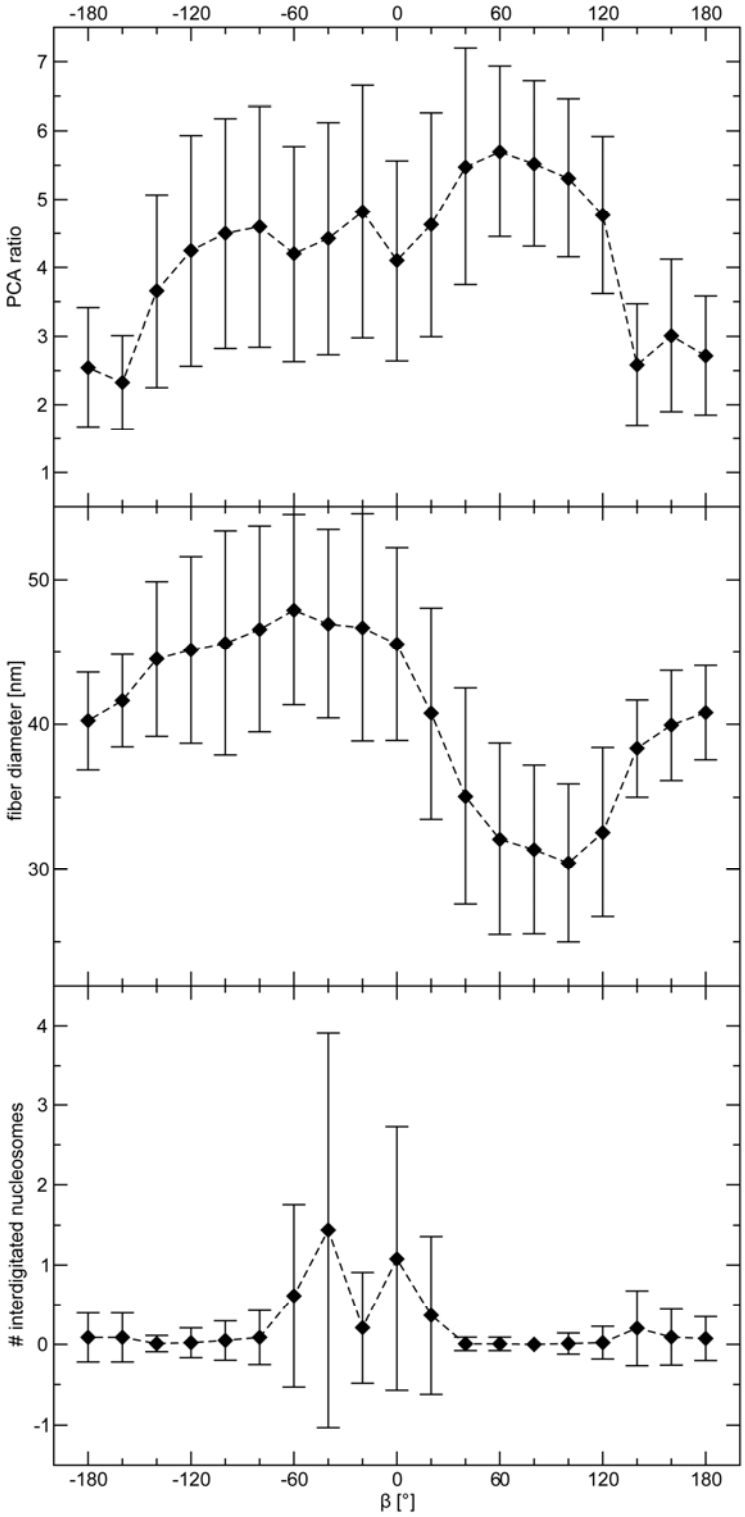

FIGURE S3. Variation of the twist angle β between consecutive nucleosomes for chicken erythrocyte chromatin. The simulations were conducted with $\alpha = 26°$, NRL = 212 bp and $E_{max} = 6\ kT$. The PCA ratio, the fiber diameter and the number of interdigitated nucleosomes are plotted. The error bar indicates the standard deviation. The PCA ratio indicated a maximum for a β value of 60° and the radius exhibited a minimum of ~30.5 nm at $\beta = 100°$. The FSC indicated a plateau in the interval of 40 – 120° and for the linear mass density a peak at $\beta = 120°$ was observed.

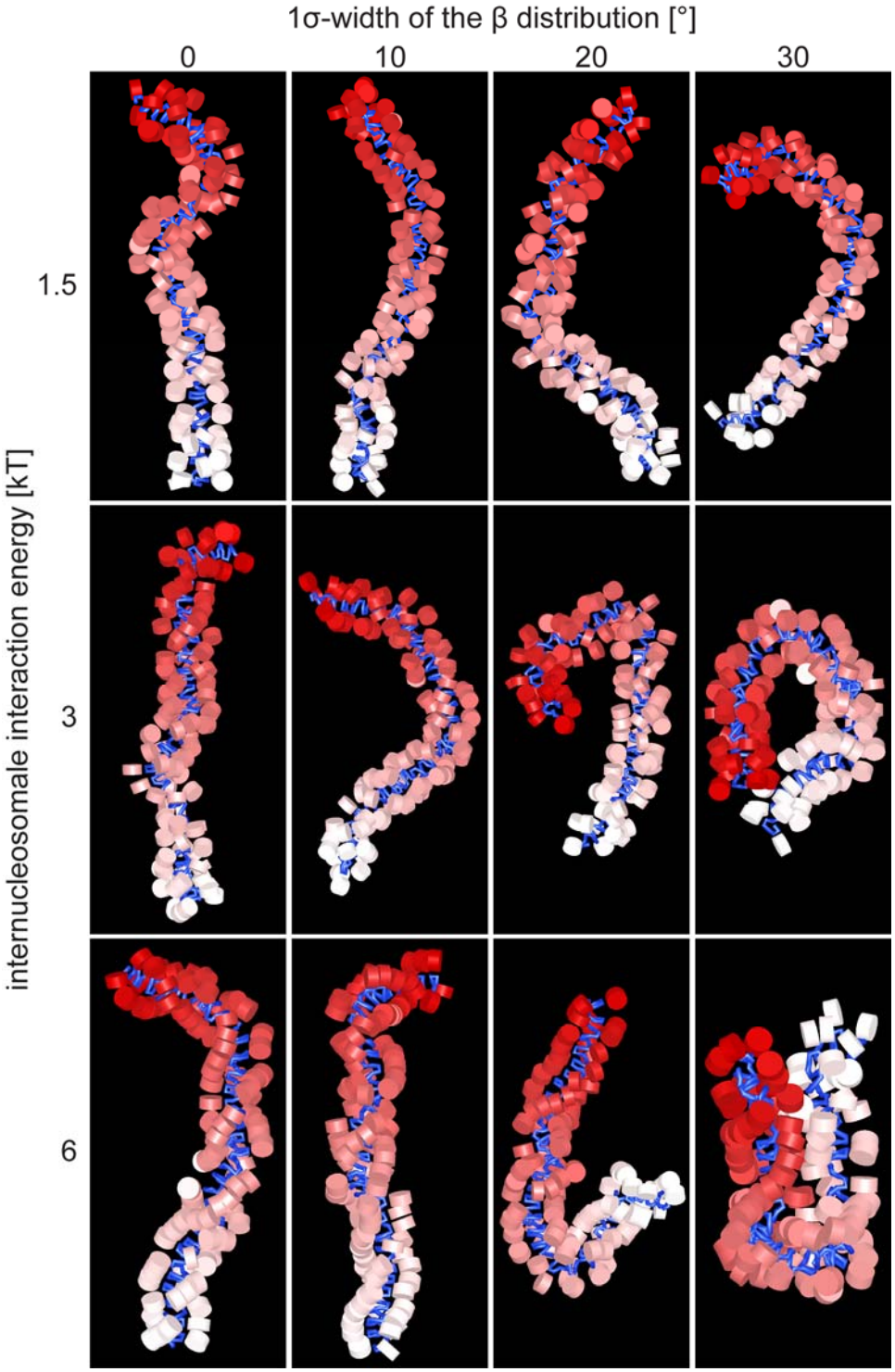

FGURE S4. Visualizations of simulated structures with Gaussian-distributed β for E_{max} values of 1.5, 3 and 6 kT. The nucleosomes are colored by their position in the chain (first is white, last is red) and the DNA segments are colored blue. The simulations were conducted with α = 26° and NRL = 212 bp. The β values between consecutive nucleosomes were Gaussian-distributed around 100° with a 1σ-width of 0° (constant beta), 10°, 20° and 30°. At higher distribution width the structures exhibited a more irregular structure and were more often bended.

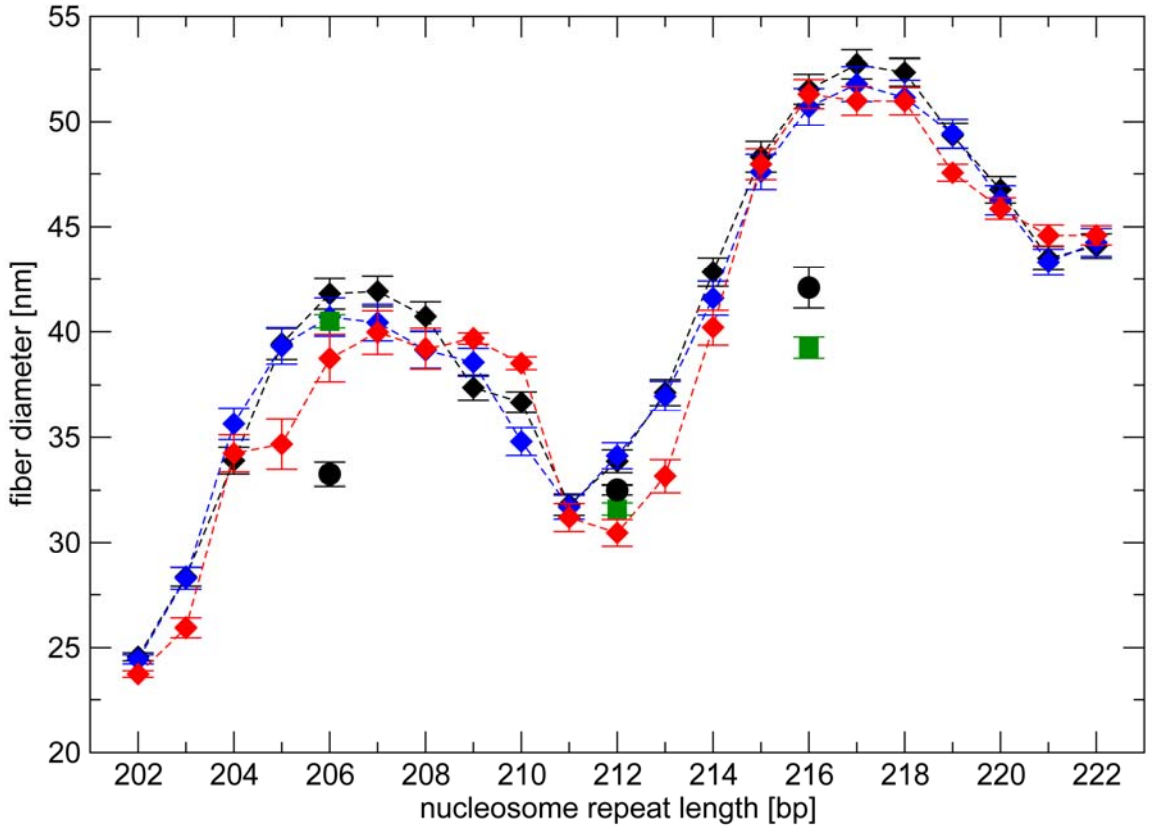

FIGURE S5. The fiber diameter as a function of the NRL for E_{max} of 1.5 (black diamond), 3 (blue diamond), 6 (red diamond), 9 (green square) and 12 kT (black circle). Error bars indicate the 95% confidence interval of the mean values. The chicken chromatin conformation was investigated for NRLs varied in one base pair intervals. The value of β was increased by 36° for each base pair added and decreased by 36° for each base pair removed. The fiber diameter indicated minima in a distance of ~10 bp at 202, 212, 222 bp with ~24, ~30 and ~44 nm, respectively.